Stem Cell Reports
Article

ISSCR

OPEN ACCESS

iPSC culture expansion selects against putatively actionable mutations in the mitochondrial genome

Maike Kosanke,[1] Colin Davenport,[2] Monika Szepes,[1] Lutz Wiehlmann,[2] Tim Kohrn,[1] Marie Dorda,[2] Jonas Gruber,[1] Kaja Menge,[1] Maike Sievert,[1] Anna Melchert,[1] Ina Gruh,[1] Gudrun Göhring,[3] and Ulrich Martin[1,*]

[1]Leibniz Research Laboratories for Biotechnology and Artificial Organs (LEBAO), Department of Cardiothoracic, Transplantation and Vascular Surgery, REBIRTH - Research Center for Translational Regenerative Medicine, Hannover Medical School, 30625 Hannover, Germany; Biomedical Research in Endstage and Obstructive Lung Disease (BREATH), Member of the German Center for Lung Research (DZL), 30625 Hannover, Germany
[2]Research Core Unit Genomics, Hannover Medical School, 30625 Hannover, Germany
[3]Institute of Human Genetics, Hannover Medical School, 30625 Hannover, Germany
*Correspondence: martin.ulrich@mh-hannover.de
https://doi.org/10.1016/j.stemcr.2021.08.016

SUMMARY

Therapeutic application of induced pluripotent stem cell (iPSC) derivatives requires comprehensive assessment of the integrity of their nuclear and mitochondrial DNA (mtDNA) to exclude oncogenic potential and functional deficits. It is unknown, to which extent mtDNA variants originate from their parental cells or from *de novo* mutagenesis, and whether dynamics in heteroplasmy levels are caused by inter- and intracellular selection or genetic drift. Sequencing of mtDNA of 26 iPSC clones did not reveal evidence for *de novo* mutagenesis, or for any selection processes during reprogramming or differentiation. Culture expansion, however, selected against putatively actionable mtDNA mutations. Altogether, our findings point toward a scenario in which intracellular selection of mtDNA variants during culture expansion shapes the mutational landscape of the mitochondrial genome. Our results suggest that intercellular selection and genetic drift exert minor impact and that the bottleneck effect in context of the mtDNA genetic pool might have been overestimated.

INTRODUCTION

Genomic instability of human induced pluripotent stem cells (iPSCs) that may cause loss of function and tumorigenic potential of their derivatives is considered as one major hurdle on the path toward clinical application (Andrews et al., 2017; Weissbein et al., 2014; Yoshihara et al., 2017). The majority of research addressing this issue is focusing on the investigation of genomic stability of the nuclear genome. However, a part of a cell's genetic information, including 13 proteins of the electron transport chain (ETC) essential for oxidative phosphorylation (OXPHOS) and 24 RNAs, is encoded in the mitochondrial genome (Clayton, 1991). Mutations of those highly conserved genes are the cause of a variety of human diseases, especially affecting tissues with high energy demand (Park and Larsson, 2011).

The mitochondrial genome exhibits a polyploid set with a few hundred up to thousands of 16.6 kb large circular mitochondrial DNA (mtDNA) molecules that are continuously replicated independently of the cell cycle (Clayton, 1991). The existence of multiple mtDNA copies per cells allows a phenomenon called heteroplasmy, which describes the simultaneous existence of wild-type and mutated mtDNA molecules in a cell. Conversely, the state when only one mtDNA genotype is present in a cell is defined as homoplasmy. However, the mtDNA composition and mitochondria network are not fixed but subjected to permanent flux and also, during cell division, the segregation of mutated and wild-type mtDNA molecules to cell progenies can also be unequal. Hence, it is not surprising that, during reprogramming, clonal iPSC lines derived from the same parental cell population were observed to harbor different variants and heteroplasmy levels (Cherry et al., 2013; Folmes et al., 2013; Kang et al., 2016; Perales-Clemente et al., 2016; Prigione et al., 2011; Yokota et al., 2015; Zambelli et al., 2018). This unequal segregation of heteroplasmies during reprogramming might arise from three sources acting on an inter- and intracellular level with different forces depending on the external conditions, namely (1) *de novo* mutations (Deuse et al., 2019; Kang et al., 2016; Prigione et al., 2011), (2) genetic mosaicism in parental cell population leading to genetically distinct iPSC clones, and (3) random allele drift during genetic bottleneck (Floros et al., 2018; Perales-Clemente et al., 2016; Zambelli et al., 2018). Several recent studies report nuclear reprogramming as the cause of *de novo* mtDNA mutations in iPSCs (Deuse et al., 2019; Kang et al., 2016; Prigione et al., 2011). However, Payne et al. (2013) introduced the concept of "Universal Heteroplasmy" demonstrating that mosaicism of heteroplasmic mtDNA variants in somatic cells, albeit at low levels (<1%), appears to be a universal finding among healthy individuals. Accordingly, many reports show evidence that the majority if not all mtDNA variants in iPSCs are pre-existing in individual somatic parental cells and arise from this mosaicism in the corresponding parental cell population (Perales-Clemente et al., 2016; Zambelli et al., 2018).

 © 2021 The Authors.
This is an open access article under the CC BY-NC-ND license (http://creativecommons.org/licenses/by-nc-nd/4.0/).

During reprogramming, somatic mitochondria are largely replaced by immature mitochondria resembling organelle morphology and distribution in embryonic stem cells (ESCs), and metabolism is switching toward glycolysis (Ma et al., 2015; Prigione et al., 2010). During this process, mtDNA copy number per cell is reduced, which is assumed to lead to a genetic bottleneck (Cao et al., 2009; Hamalainen et al., 2013). Such a reduction in mtDNA pool increases the effect of random genetic drift on mtDNA segregation within a cell and between cell offspring during cell division (Aryaman et al., 2019; Roze et al., 2005). However, at the same time this bottleneck might expose mutations to selective forces, and subtle selective pressures can exert maximal impact (Floros et al., 2018; Hamalainen et al., 2013; Roze et al., 2005; Wei et al., 2019). As of yet, it is not understood to what extent the segregation is driven by random allele drift or selection (Zambelli et al., 2018).

In contrast to the nuclear genome, selection on mutated mtDNA molecules can act on an intercellular or intracellular level. On the intercellular level, genetically encoded inequalities in cell fitness of parental cells can lead to eliteness of cells to attain iPSC state and their dominance in the reprogramming niche (Kosanke et al., 2021; Shakiba et al., 2019). However, high mutational burden or pathogenic mutations in specific mtDNA regions can also hinder reprogramming (Floros et al., 2018; Hung et al., 2016; Kang et al., 2016; Latorre-Pellicer et al., 2016; Wahlestedt et al., 2014; Yokota et al., 2015).

On the intracellular level, certain mtDNA variants can be selected (Latorre-Pellicer et al., 2016). As mtDNA molecules are uniparentally inherited and the mutation rate is 6- to 20-fold higher than that of genomic DNA (Naue et al., 2015), theoretically, without a repair mechanism, mtDNA would continuously accumulate mutations ultimately ending in a "mutational meltdown" called Muller's ratchet (Chinnery and Prudent, 2019; Floros et al., 2018). To avert this, during female germline development and early embryogenesis, fragmentation of mitochondria and mitochondrial selective autophagy (mitophagy) purges mutated mtDNA and mitochondria (Chinnery and Prudent, 2019; Floros et al., 2018; Kandul et al., 2016; Latorre-Pellicer et al., 2016; Lieber et al., 2019). As iPSCs experience rejuvenation to an ESC-like state (Prigione et al., 2010), a similar mechanism might act during reprogramming that leads to mitophagy of damaged organelles or reduced segregation of such (Floros et al., 2018).

During prolonged culture of iPSCs, genetic drift and selection continue to form the mutational landscape of the mitochondrial genome. Although most studies report that mtDNA variants did not experience any substantial change of heteroplasmy level during long-term culture, there is also evidence for both positive (Deuse et al., 2019; Zambelli et al., 2018) and negative selection of mtDNA variants (Cherry et al., 2013; Folmes et al., 2013; Perales-Clemente et al., 2016), without clear comprehension of the causes or mechanisms. On one hand, mitochondrial heteroplasmic variants were observed to arise in or dominate human iPSC and ESC lines during prolonged culture (Deuse et al., 2019; Maitra et al., 2005; Zambelli et al., 2018). Notably, single-cell analysis has revealed heterogeneous heteroplasmies among cell populations and there was no indication of selection against potentially pathogenic variants during culture (Zambelli et al., 2018). On the other hand, various studies reported that extended passaging of iPSC clones with high level of heteroplasmy affecting specific genes led to reduction of mutant mtDNA (Cherry et al., 2013; Folmes et al., 2013; Hamalainen et al., 2013; Latorre-Pellicer et al., 2016; Perales-Clemente et al., 2016).

It is, however, currently unknown on which scale the diverse mechanisms shape the mutational landscape of mtDNA. We have, therefore, evaluated to what extent and at which stage random genetic drift and selection might act. To this end, we have analyzed 26 clonal iPSC lines and their corresponding parental cell populations by mtDNA sequencing and determination of their copy number to gain insight into the dynamics and mechanism behind mtDNA segregation during reprogramming, prolonged culture, and differentiation.

RESULTS

No evidence for clonal eliteness or mutation clearance mechanisms during reprogramming

To analyze the effect of reprogramming on mtDNA segregation and mutational landscape, we generated 26 clonal iPSC lines of early passages of endothelial cells (ECs) of 6 neonatal (human umbilical vein EC [hUVEC]) and 4 aged donors (human saphenous vein ECs [hSVEC]; age 64–88 years). To assess inter-clonal differences, 3 iPSC clones were derived per donor, with the exception of D#6 hUVEC and D#40 hSVEC, for which only one clone each was analyzed. In contrast to prior assumptions, mtDNA copy number in early passage iPSCs (p4-9) was, with, on average, 1,252 mtDNA copies per cell, similar to ECs of the corresponding parental cell populations (~1,114 copies per cell at ~ p4) and ESCs (~934 mtDNA copies per cell) (Figure 1A). Although there was no distinct reduction and, hence, bottleneck in mtDNA copy number in iPSCs compared with their parental cells, the mitochondria network was remodeled to a more immature state with mitochondria being punctual and located in the perinuclear region (Figure S1), as described previously (Prigione et al., 2010).

mtDNA of early passages of iPSCs (mean p6.5) and the corresponding parental cell populations, at a similar

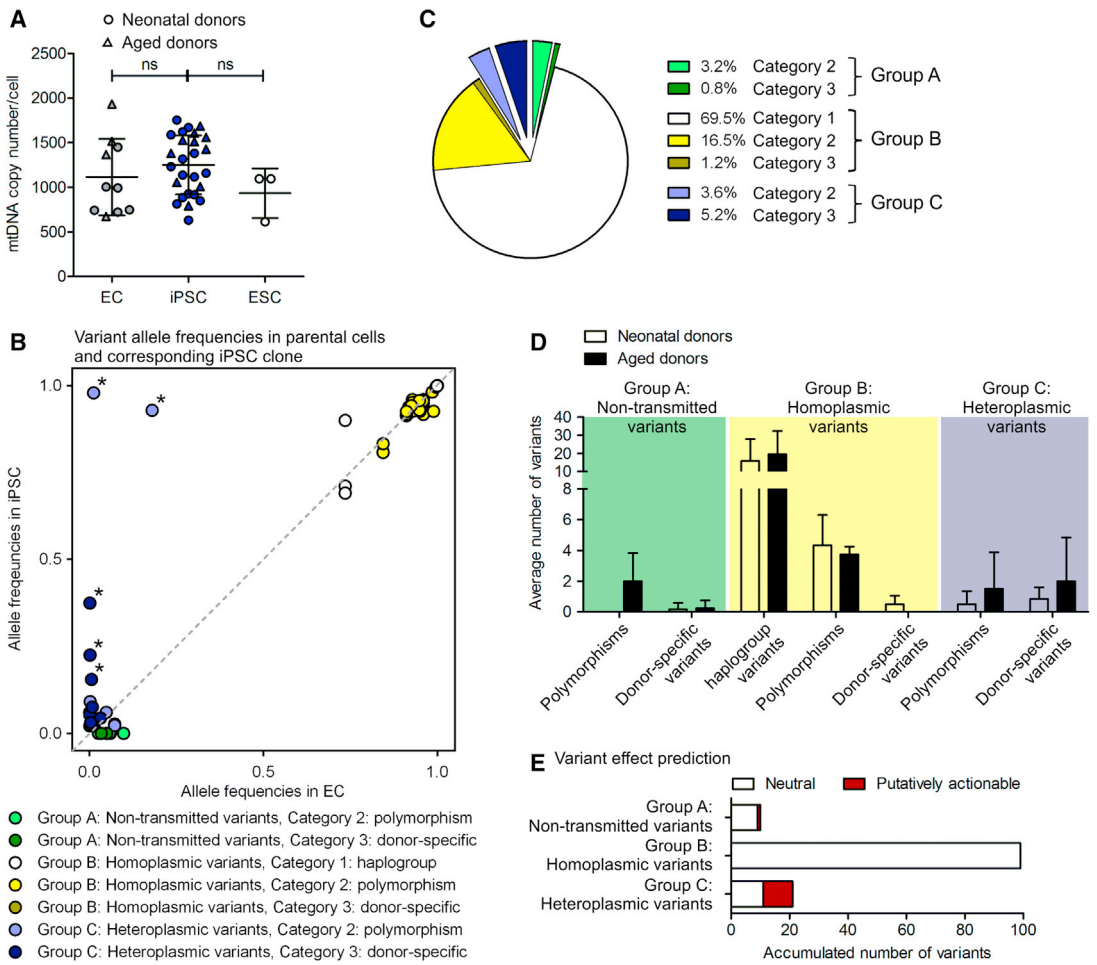

Figure 1. Characterization of mtDNA copy numbers and mtDNA variants in iPSCs and their parental cells

(A) Average mtDNA copy number per cell in parental endothelial cells (ECs), EC-derived iPSC clones, and ESC lines. EC N = 10 donors; iPSC N = 26 early passage clones; ESC N = 3 lines; each with 1–5 biological replicates. One-way ANOVA with Tukey's multiple comparison test.

(B) Corresponding allele frequencies (AFs) of all variants in iPSC clones and parental cell populations detected by mtDNA sequencing of 26 early passage iPSC clones and their corresponding 10 parental cell populations. Group A non-transmitted variants were detected only in parental cell populations (AF > 0.02). Group B homoplasmic variants in parental cell population and iPSCs derived thereof. Group C heteroplasmic variants detected in an iPSC clone with AF > 0.02 but less frequent in parental cell population. Category 1 comprises haplotype variants, category 2 polymorphisms defined by a population frequency $\geq$ 0.02, and category 3 variants that are specific to a donor. N = 10 donors.

(C) Proportion of variant groups and categories of all variants. N = 10 donors.

(D) Average number of variants per group and category in iPSC clones and/or corresponding parental cell population of neonatal and aged donors. Neonatal donors N = 6 donors with 16 iPSC clones; aged donors N = 4 donors with 10 iPSC clones. Displayed is mean with SD. *Group C (heteroplasmic) variants with heteroplasmy level above 10% (AF > 0.1) in iPSCs.

(E) Effect of variant on gene functionality was predicted based on a consensus of *in silico* prediction algorithms (snpEff impact, CADD, Condel, and HmtVar). Graph displays ratio of variants with neutral and putatively actionable prediction within group A (non-transmitted), group B (homoplasmic), and group C (heteroplasmic). N = 10 donors.

passage as subjected to reprogramming (mean p4.5), was sequenced. Analysis of mtDNA variants in iPSCs and ECs revealed three groups. Group A, non-transmitted variants, includes variants detected only within the parental cell populations that were not transmitted to any iPSC clone of the representative donor (detection limit allele frequency [AF] 0.02). In contrast, groups B and C contain transmitted variants with group B variants being homoplasmic in iPSC clones, and their corresponding parental cell populations and group C variants being heteroplasmic and detected in one iPSC clone per donor only (Figure 1B; Tables 1 and S1). The heteroplasmies are defined for every

Table 1. Number of mtDNA variants in iPSC clones and corresponding parental cell populations

		Non-transmitted (group A)		Transmitted (groups B + C)				
				Homoplasmic (group B)			Heteroplasmic (group C)	
Donor	Haplogroup	Polymorphisms (cat. 2)	Donor specifi (cat. 3)	Haplogroup variants (cat. 1)	Polymorphisms (cat. 2)	Donor specific (cat. 3)	Polymorphisms (cat. 2)	Donor specific (cat. 3)
D#1 hUVEC	H7a1	0	0	9	3	0	0	1
D#2 hUVEC	H1c3	0	0	10	5	1	0	0
D#3 hUVEC	H2a1c	0	1	7	3	0	2	2
D#4 hUVEC	J1c8a	0	0	28	3	1	1	1
D#5 hUVEC	J1b1a3	0	0	34	8	1	0	0
D#6 hUVEC	H87	0	0	7	4	0	0	1
Neonatal donors	mean	0.0	0.2	15.8	4.3	0.5	0.5	0.8
D#31 hSVEC	H1c2	4	0	9	4	0	0	2
D#37 hSVEC	H10b	0	0	8	3	0	4	6
D#38 hSVEC	I3	3	0	32	4	0	1	0
D#40 hSVEC	J1c5a	1	1	29	4	0	0	0
Aged donors	mean	2.0	0.3	19.5	3.8	0.0	1.3	2.0
Total	mean	**0.8**	**0.2**	**17.3**	**4.1**	**0.3**	**0.8**	**1.3**
	sum	8	2	73	23	3	8	13

variant separately as the percentage of variant allele count per total allele count at the variant locus (= AF × 100). Although, in most cases the AF of those variants within the parental cell population was below the general detection limit of 0.02, careful assessment of variants within their genomic context taking local error rates in account allowed us to confirm pre-existence of more than half of the variants with statistical confidence ($p = 0.05$) (Table S2) (see experimental procedures). We could not prove pre-existence of the other half of variants with statistical confidence (Table S2, indicated by value in brackets), but previous reports also support our assumption that most of these variants arose from the parental cell population (Perales-Clemente et al., 2016; Zambelli et al., 2018).

Variants of each group can be further categorized: category 1, haplotype variants, are variants that define the haplogroup of every donor. Category 2 variants comprise polymorphisms defined by a population frequency of the variant (NCBI GenBank frequency [GB]) > 0.02. Category 3 variants are unique to a donor and rare in human populations and, are, therefore, called hereafter donor-specific variants (Tables 1 and S1).

Group B (homoplasmic) variants, mainly haplotype variants or polymorphisms (category 1 and 2), represent the vast majority of all variants (>87%) detected in mtDNA. Almost 9% of variants in iPSCs were heteroplasmic (group C) variants that were typically rare among the parental cell population and mainly categorized as donor specific (category 3) (Figure 1C; Table 1).

In contrast to Kang et al. (2016), but in accordance with Payne et al. (2013), we did not observe a dependency of overall mitochondrial mutational load of iPSCs with donor age (Figure 1D; Table 1), which might be partly attributed to different source tissue. Moreover, on average, aged donors tended toward a slightly higher number of group A (non-transmitted) and C (heteroplasmic) variants, indicating higher mosaicism as reported by previous studies (Naue et al., 2015).

Next, we analyzed the functional consequences of variants to evaluate to which extent clonal eliteness or negative selection might impact their transmission from parental cells to iPSC clones. Variant effect prediction based on a consensus of *in silico* prediction algorithms revealed that all group B (homoplasmic) variants and 90% of group A (non-transmitted) variants are neutral (Figure 1E). Strikingly, almost 48% of the group C (heteroplasmic) variants in iPSCs are putatively actionable, suggesting that mtDNA segregation during reprogramming does not act selectively against potentially damaging mutations. However, while we cannot exclude positive selection, we also found no direct evidence for enrichment of individual mutations or any mutational hotspot in specific genes during reprogramming.

Notably, the heteroplasmy level of the group C (heteroplasmic) variants was generally low (below 10%; AF < 0.1) in iPSCs with the exception of five variants (Figure 1B, marked with *). While two of these five variants were neutral polymorphisms with very high heteroplasmy levels >90% (AF > 0.9) in individual iPSC clones, the other three variants were putatively actionable donor specific with intermediate heteroplasmy levels of 16%–38% (AF 0.16–0.38) in single iPSC clones, affecting NADH dehydrogenase (ND) *ND4* and *ND5* genes of the ETC complex I. Interestingly, complex I, in particular *ND5*, is frequently mutated in diverse diseases and cancer (Copeland et al., 2002). However, our data do not allow any conclusion whether the affected iPSC clones simply represent stochastic events, where iPSC clones were derived from rare parental cell clones with increased heteroplasmy levels, or whether positive selection processes occurred. Anyway, we could not observe altered mitochondrial features or metabolic functionality of the *ND5* mutations in affected iPSC clones (D#3 hUVEC C2 with 38% m.13099G > A and D#37 hSVEC C10 with 23% m.12686T > C) (Figure S2, marked with *) compared with their sister clones (D#3 hUVEC C1 and D#37 hSVEC C4) derived from the same parental cell population. All iPSC clones displayed a similar proliferation rate measured as population doubling, mtDNA copy number per cell, specific yield coefficient of lactate per glucose molecule, mitochondrial content, mitochondrial membrane potential, and reactive oxygen species (ROS) content, as well as similar expression of genes involved in metabolism (*mTOR*, *ND5*, *PDK1*, *PGC1a*, *PGC1b*, *PRKAA1*) (Figure S2). Also, genes of mtDNA replication and transcription (*POLG2*, *TFAM*, *NRF1*), mitochondria dynamics (*MFN1*, *OPA1*, *DNML1*), and mitophagy (*PINK1*, *PRKN*) were not differentially expressed between non-mutated and mutated iPSC clones, although they were overall significantly higher expressed in iPSCs compared with their parental cells (Figure S2F). As iPSC metabolism is not predominantly based on OXPHOS and the heteroplasmy rates were only 23% and 38%, this result is not unexpected and, in accordance to observations of previous work (Hamalainen et al., 2013; Perales-Clemente et al., 2016; Wahlestedt et al., 2014; Yokota et al., 2015), also decreases the likelihood of a clonal eliteness on the intercellular level during reprogramming.

Prolonged culture expansion leads to clearance of putatively actionable mtDNA mutations

There are contradictory reports regarding the propagation of mtDNA mutations during prolonged culture. While some studies report increase and dominance (Deuse et al., 2019; Maitra et al., 2005; Zambelli et al., 2018), other studies observed a reduced proportion of mutated mtDNA during culture (Cherry et al., 2013; Folmes et al., 2013; Perales-Clemente et al., 2016). Seven of the iPSC clones that had been analyzed in an early passage were also sequenced in later passages p30 and p50 to trace the dynamic of mtDNA heteroplasmies during culture expansion.

It is noteworthy that 86% of the group C (heteroplasmic) variants detected in later passages were also detectable in early iPSC passages and/or the corresponding parental cell population with statistical confidence (p = 0.05). The remaining variants were apparently present in the parental cells and early passages, too, but could not be confirmed with statistical confidence (p = 0.05). Hence, although we cannot exclude it, we also did not observe substantial evidence for *de novo* mutagenesis during prolonged culture expansion (Table 2).

Investigation of the regions affected by mutations showed that around 60% of group C (heteroplasmic) variants were located in coding regions (Figure 2A, black) and, therefore, affected coding regions more frequently than group A (non-transmitted) and group B (homoplasmic) variants. Furthermore, compared with group A and B variants which constitute almost entirely nucleotide transitions (transition/transversion ratio [Ts/Tv] > 30), group C (heteroplasmic) variants are characterized by lower T > C transitions compared with C > T and by higher proportion of transversion events (Ts/Tv 3.4) (Figure 2B). Both C > T and T > C substitutions are described as the predominant type of substitution in homoplasmic variants originating from germline transmission (Naue et al., 2015; Wei et al., 2019). The mutational signatures of heteroplasmic group C variants seems to be mainly shaped by the same mechanism; however, abundance of other substitution events suggest an additional origin, such as EC culture expansion or tissue mosaicism of those variants. Consequently, group C mutations would, therefore, never have been subjected to the control and repair mechanisms acting during mtDNA transmission in germ cells.

Depending on the dynamic of mtDNA mutation progression during culture expansion, all group C variants in iPSCs were divided into four groups, namely enriched, stable, depleted, and fluctuating variants (Table 2, illustrated by the changes in blue shades). While enriched variants are defined as such that increased in AF over iPSC expansion culture more than 10-fold (average 76-fold; range 11- to 250-fold), stable variants did not change their AF during iPSC expansion culture (average fold change between passages 1.03; range 0.67–1.49; SD 0.25). Depleted variants were reduced in AF from the early or intermediate passage to the late one by more than 10-fold (average 64-fold; range 15- to 225-fold) (Table 2). The group of fluctuating variants incorporates basically variants that might be also added to one of the above-mentioned groups, but as their fold change over culture only ranged from 2.7- to 8.8-fold (average 4.7; SD 2.2), we decided not to include them. A

Table 2. Group C mtDNA variant heteroplasmy levels change during iPSC culture expansion

Variants	Consequence	Gene Symbol		Donor	iPSC clone	AF EC	AF p 6	AF p 30	AF p 50	Fold change
Enriched										
m.1226C>T	RNA coding	MT-RNR1		D#37 hSVEC	C8	0.008	0.004	0.055	0.144	35.9
m.1884G>A	RNA coding	MT-RNR2		D#37 hSVEC	C8	(0.006)	(0.004)	0.920	0.999	249.8
m.3975C>A	missense	MT-ND1		D#3 hUVEC	C1	0.001	(0.001)	0.006	0.085	84.8
m.10586G>A	synonymous	MT-ND4L		D#3 hUVEC	C1	(0.003)	(0.005)	0.010	0.083	16.5
m.15640C>T	synonymous	MT-CYB		D#37 hSVEC	C10	0.008	0.016	0.062	0.179	10.9
m.16147C>T	regulatory region			D#2 hUVEC	C2	(0.001)	(0.015)	0.095	0.877	58.5
Stable										
m.72T>C	regulatory region			D#3 hUVEC	C2	0.181	0.929	0.999	1.000	1.0
m.297A>C	regulatory region			D#37 hSVEC	C4	(0.013)	0.022	(0.025)	(0.039)	1.1
m.366G>A	regulatory region			D#37 hSVEC	C8	0.049	0.061	0.041	0.061	1.1
m.5192A>C	synonymous	MT-ND2		D#3 hUVEC	C1	0.013	0.019	0.026	0.022	1.0
m.5894_5895insC	regulatory region			D#37 hSVEC	C10	0.012	0.979	0.981	0.953	1.0
m.13099G>A	missense	MT-ND5		D#3 hUVEC	C2	0.002	0.374	0.376	0.423	1.0
Depleted										
m.8964C>T	synonymous	MT-ATP6		D#38 hSVEC	C9	(0.001)	0.061	0.008	0.004	14.5
m.10946_10947insC	frameshift	MT-ND4		D#37 hSVEC	C8	0.006	0.155	0.021	0.010	15.9
m.12020C>T	missense	MT-ND4		D#37 hSVEC	C10	0.011	0.026	0.014	0.001	23.0
m.12686T>C	missense	MT-ND5		D#37 hSVEC	C10	(0.002)	0.225	0.087	(0.001)	225.1
m.15575G>A	missense	MT-CYB		D#37 hSVEC	C4	0.010	0.038	0.014	(0.001)	38.5
m.3800T>A	missense	MT-ND1		D#3 hUVEC	C1	(0.004)	(0.007)	0.028	(0.001)	28.3
m.10569G>A	missense	MT-ND4L		D#3 hUVEC	C2	(0.003)	0.012	0.104	0.005	22.5
m.13216A>G	missense	MT-ND5		D#2 hUVEC	C2	(0.001)	0.019	0.029	(0.000)	143.8
Fluctuating										
m.4193T>C	missense	MT-ND1		D#3 hUVEC	C1	0.032	0.044	0.023	0.016	2.7
m.16256C>T	regulatory region			D#37 hSVEC	C4	(0.003)	0.091	0.015	0.019	4.8
m.225G>T	regulatory region			D#2 hUVEC	C2	0.010	0.014	0.038	0.010	3.8
m.5450C>T	synonymous	MT-ND2		D#3 hUVEC	C2	0.010	0.029	0.034	0.085	2.9
m.6316A>C	missense	MT-CO1		D#37 hSVEC	C4	0.013	0.022	0.029	0.061	2.7
m.8660C>T	missense	MT-ATP6		D#37 hSVEC	C4	(0.007)	0.028	0.302	0.241	8.8
m.12147G>A	RNA coding	MT-TH		D#2 hUVEC	C2	0.007	0.012	(0.007)	0.083	6.8
nd in p30-50										
m.1602C>T	RNA coding	MT-TV		D#6 hUVEC	C5	(0.001)	0.021			
m.6255G>A	missense	MT-CO1		D#31 hSVEC	C1	(0.001)	0.054			
m.8816A>T	missense	MT-ATP6		D#31 hSVEC	C1	(0.009)	0.076			
m.11571T>C	missense	MT-ND4		D#4 hUVEC	C3	(0.003)	0.025			
m.13077C>T	synonymous	MT-ND5		D#1 hUVEC	C5	(0.004)	0.031			
m.16189T>C	regulatory region			D#4 hUVEC	C1,C3	0.0728	~0.025			

Effect prediction:	Allele frequencies:
Putatively actionable	0.02-0.05
Neutral	0.05-0.1
	0.1-0.5
	0.5-1

(); existence of variant in parental cell population or iPSC clone not confirmed with statistical confidence ($p > 0.05$).

last group of variants (named "nd in p30-50") shown in Table 2 comprises those iPSC-enriched variants that were found in iPSC clones that were only analyzed at early passage.

Among the entirety of group C (heteroplasmic) variants (AF > 0.02), all enriched variants were predicted to be neutral as well as 83% of the stable variants. The group of fluctuating variants or those not analyzed in high passages (nd in p30-50) contained 43%–50% putatively actionable variants (Figure 3A). Most interestingly, 88% of putatively actionable variants was observed among the depleted variants. Focusing only on group C (heteroplasmic) variants

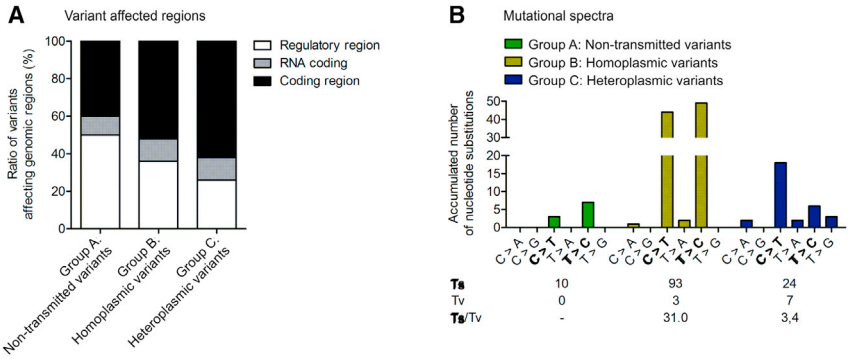

Figure 2. Transmitted heteroplasmic group C variants affect coding regions more frequently and are characterized by a higher transversion rate

Twenty-six iPSC clones at an early passage, with 7 of these additionally at later passages, as well as the corresponding parental cell population of the total 10 donors, were subjected to mtDNA sequencing. All variants were classified into three groups. Variants of group A, non-transmitted variants, were detected only in parental cell populations. Group B variants were homoplasmic in parental cell population and iPSCs derived thereof. Group C, heteroplasmic variants, were detected in iPSC clones with AF > 0.02 at any passage but were less frequent in the corresponding parental cell population. N = 10 donors.

(A) Total number of non-transmitted, homoplasmic, and heteroplasmic variants that affected regulatory, RNA coding, or coding regions.

(B) Mutational spectra. Ts, transition; Tv, transversion. Transitions are marked in bold.

with intermediate heteroplasmy levels (AF > 0.1, which equals an averaged heteroplasmy level of >10%), yielded similar results, although the sample size of such was quite small (Figure 3B). In general, donor age did not affect the genetic stability or clearance mechanisms as, in all groups (enriched, stable, depleted, and fluctuating), heteroplasmic group C variants are equally apportioned in neonatal (hUVEC) and aged (hSVEC) donors (Table 2). Furthermore, karyotype analysis performed for D#3 hUVEC C2, D#37 hSVEC C10, and control clone D#3 hUVEC C1 demonstrated that clones maintained normal karyotypes over time in culture (Table S3). However, we did not analyze for smaller chromosomal aberration.

It is assumed that iPSCs are subjected to a genetic bottleneck when the mtDNA copy number per cell is reduced in the pluripotent state compared with somatic cells. It is still controversially discussed, however, whether random genetic drift during this bottleneck or selection processes are responsible for the observed changes in heteroplasmy levels during prolonged iPSC culture expansion (Aryaman et al., 2019; Hamalainen et al., 2013). Notably, we did not observe any strong reduction in the mtDNA copy number in iPSCs compared with ECs of the parental cell populations (Figure 1A). Furthermore, the mtDNA copy number per iPSCs stayed constant during prolonged iPSC expansion culture (Figure 3C).

Here, we applied a neutral model of mtDNA genetic dynamics of Aryaman et al. (2019) to understand how distribution of heteroplasmies evolves over time without selection. Therefore, this model was utilized as a null hypothesis to assess whether random genetic drift by itself is sufficient to explain the observed changes in heteroplasmy levels, or whether additional selection factors play a role. The model of Aryaman et al. was developed for prediction of a possible change in heteroplasmy level of one mutated allele in a post-mitotic cell with mtDNA undergoing turnover. This means that degradation and replication of mtDNA occurs to the same extent over time, allowing the ratio of mutated allele to fluctuate. Although our culture consists of mitotic iPSCs and requires frequent cell culture splitting, we applied this model here under the assumptions that (1) iPSCs experience symmetric division and equal segregation and expansion of all mtDNA molecules and (2) the effect of random gene drift during iPSC culture passaging is negligible. A more complex model predicting dynamics and selection in a unicellular life cycle with bottleneck and expansion in a multi-cellular organism (Roze et al., 2005) confirms that these assumptions prove valid for our population size (cells in culture before and after splitting). The model of Aryaman et al. includes, in addition, a fragmentation factor, which indicates the ratio of fused mitochondria. As unfused, punctuated mitochondria are a typical feature of iPSCs (Figure S1), we excluded this factor in our modeling. The rate of turnover of mtDNA molecules and also selective mitophagy is set in this model by the factor μ (mitophagy rate). This factor is equivalent to a selection coefficient in other models (Roze et al., 2005).

Determination of mtDNA content has shown that the mtDNA copy number stayed constant over time during iPSC culture expansion (on average ~1,000 copies/cell) (Figure 3C). Thus, we simulated the possible heteroplasmy variance over time for three different heteroplasmic group C variants exemplarily for each group of enriched, stable, and depleted variants, assuming that cells contain 1,000 mtDNA molecules and no selection is acting (Figure 3D, green line). The variance in heteroplasmy level in cultured iPSCs increases with time according to random genetic drift. However, the modeling also indicates that expectable changes in heteroplasmy due to random genetic drift without computing an additional selection coefficient are very low even over the course of 50 iPSC passages

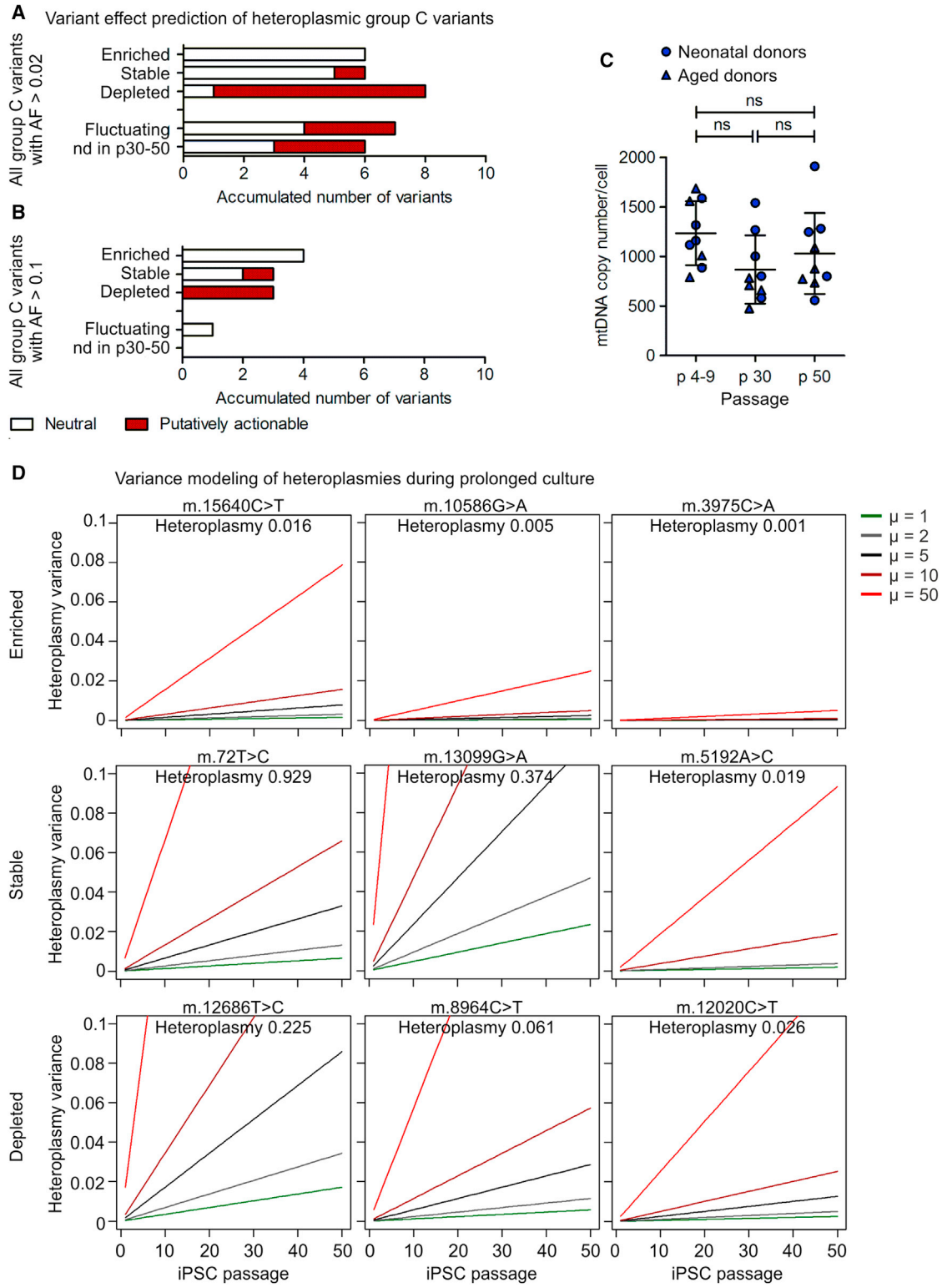

Figure 3. Prolonged culture expansion selects against putatively actionable mtDNA mutations in iPSCs

Twenty-six iPSC clones at early passage (on average p6.5) and seven of them additionally at intermediate (p30) and late passage (p50) were analyzed by mtDNA sequencing. Heteroplasmic variants (group C) were divided into the groups of enriched variants (defined as >10-fold

(legend continued on next page)

(Figure 3D, green line). Consequently, this result is consistent with the observation made in the group of stable group C variants, which proved to be unchanged over the course of time (fold change on average 1.03, Table 2). However, this simulation without additional selection factor cannot explain the observed increase or decrease in heteroplasmy levels of the enriched or depleted variants. In contrast, incorporating a selection coefficient (included as the μ factor) in the model can explain our observation. For depleted variants, a selection coefficient of μ = 10–50 (Figure 3D, dark and light red lines) was, in general, sufficient to simulate the reduction of heteroplasmies. In contrast, to reach the change in heteroplasmy level observed by enriched variants, μ > 50 would even be needed in most of the cases. Taken together, the analysis of the mtDNA copy number and modeling revealed two aspects: (1) the mtDNA copy number in iPSCs is high enough (no strong bottleneck in the pluripotent state) to prevent noteworthy effects by random genetic drift and (2) enrichment of neutral and clearance of putatively actionable group C (heteroplasmic) variants is likely caused by active selection during iPSC expansion culture.

Dynamics of mtDNA copy number during differentiation does not change variant heteroplasmy levels

To investigate the development of heteroplasmy levels during differentiation and the consequences of mtDNA mutations for differentiated iPSC derivatives, the two iPSC clones harboring intermediate level of putatively actionable *ND5* mutations (D#3 hUVEC C2 with 38% m.13099G > A and D#37 hSVEC C10 with 23% m.12686T > C) and their sister iPSC clones (D#3 hUVEC C1 and D#37 hSVEC C4) derived from the same parental cell population were differentiated into cardiomyocytes (CMs). Monitoring of the mtDNA copy number during the differentiation process, surprisingly, revealed a more complex dynamic than expected. Instead of a simple increase of mtDNA copies from iPSCs to CMs with higher metabolic demands, the general dynamic followed a process through three phases (Figure 4A). During the first phase (differentiation day [dd] 0 to dd1), starting with WNT pathway activation by CHIR99021 treatment for 24 h, mtDNA copy number per cell increased. After subsequent WNT pathway inhibition by Wnt-C59 for 48 h (dd1–dd3), mtDNA copy number per cell was reduced reaching its minimum around dd5 or dd6. After dd6 mtDNA copy number increased again to ∼dd10. The mtDNA copy number from dd10 onward stayed unchanged with, on average, 1,532 mtDNA copies per cell (Figure 4A). During reprogramming, such a bottleneck effect is suspected to exert influence on mtDNA segregation. However, analysis of heteroplasmy levels during the differentiation process by mtDNA sequencing at dd0, dd5, and dd15 of differentiation demonstrated that the heteroplasmy level of all variants stayed constant during differentiation, with an average fold change of 1.00 (range 0.83–1.15; SD 0.08) (Figure 4B), a result supported by the observations of previous work (Hamalainen et al., 2013; Zambelli et al., 2018).

Moreover, the mtDNA copy number dynamic was not influenced by the presence of the *ND5* mutations in iPSC clones D#3 hUVEC C2 or D#37 hSVEC 37 C10 (Figure 4A, marked with *). Taking into account the relatively low AF, it is, however, not unexpected that differentiation efficiency, final mtDNA copy number in CMs, and the phenotype of the mitochondria network were similar in the iPSC clones with and without the respective *ND5* mutations (Figure S3). Similarly, metabolic features measured as mitochondrial content (MitoTracker), membrane potential (tetramethylrhodamine methyl ester [TMRM]), and ROS (Brite 670) in mutated relative to wild-type iPSC-derived CMs was not significantly affected (Figure S4A). Notably, gene expression quantification demonstrated that, surprisingly, *ND5* expression was not upregulated in iPSC-derived CMs (Figure S4B). Hence, beside the relatively low heteroplasmy level of the mutations, additional low expression level of *ND5* could explain the absence of any molecular

increase in heteroplasmy level during culture), stable variants (with fold change ∼1), depleted variants (decreased by >10-fold), and fluctuating variants (change of heteroplasmy level did not allow confident classification into one of the above-mentioned groups). The group of "nd in p30-50" comprises variants that were detected in iPSC clones that were only analyzed in the early passage. The ratio of neutral and putatively actionable iPSC-enriched variants within each group was determined. Effect prediction is based on a consensus of *in silico* prediction algorithms (snpEff impact, CADD, Condel, and HmtVar).

(A) Analysis including all heteroplasmic group C variants with minimum AF 0.02 at any passage of iPSC expansion culture. N = 10 donors.

(B) Analysis including all group C variants with minimum AF 0.1 at any passage. N = 10 donors.

(C) Average mtDNA copy number per iPSC clone in different passages of culture expansion. N = 9 clones. One-way ANOVA with Tukey's multiple comparison test.

(D) Modeling of heteroplasmy variance over passages, exemplarily for three variants with high, intermediate, and low heteroplasmy levels for each group. The model for genetic drift was adapted from Aryaman et al. (2019) and allows prediction of variance of the heteroplasmy level and, therefore, possible change of the heteroplasmy levels over time. As a neutral model, it predicts heteroplasmy variance only based on random gene drift, while selection forces can be incorporated by an additional coefficient. For the different heteroplasmy levels in iPSCs with N = 1,000 mtDNA molecules, the heteroplasmy variances in a neutral situation (green line) and with selection acting with various strength (μ = 2, 5, 10, and 50) are shown.

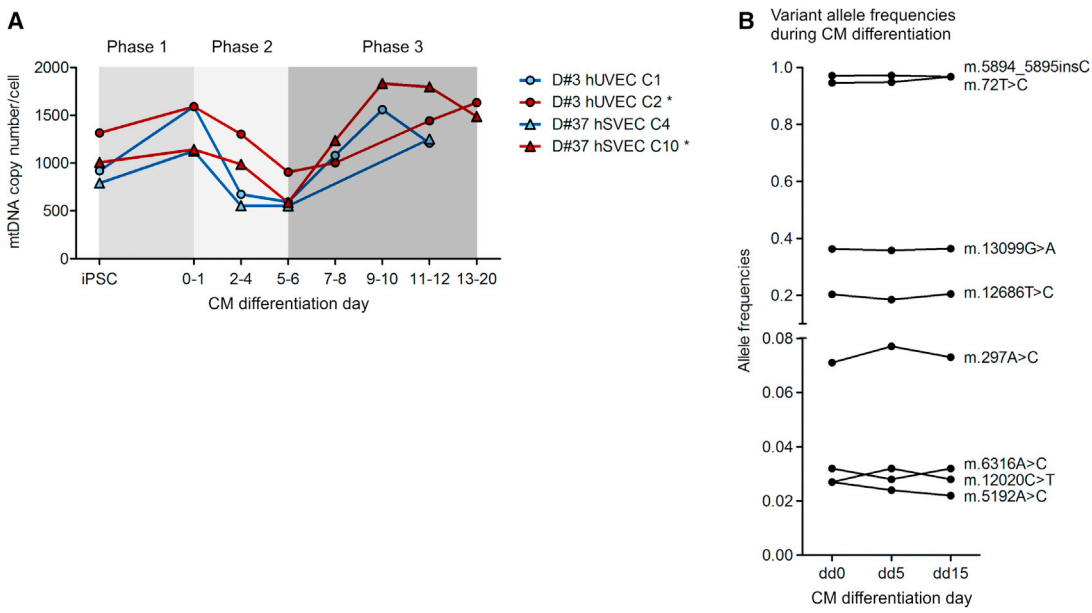

Figure 4. mtDNA content experiences reduction during cardiomyocyte differentiation without change in variant heteroplasmy levels

Two iPSC clones (D#3 hUVEC C2 and D#37 hSVEC C10) each harboring a different putatively actionable mutation in *ND5* (m.13099G > A and m.12686T > C, respectively) at intermediate heteroplasmy level and their sister iPSC clones generated from the same parental cell population were differentiated into cardiomyocytes (CMs). Mutated iPSC clones are marked with *.

(A) Average mtDNA copy number per cell during CM differentiation. N = 1–2 differentiations.

(B) At different time points during CM differentiation (differentiation day [dd] 0, dd5, and dd15), mtDNA was sequenced. Plot displays the dynamic of heteroplasmy levels during CM differentiation of heteroplasmic variants with AF > 0.02. N = 4 clones.

phenotype, at least under our differentiation conditions. Finally, bioartificial cardiac tissues (BCTs) (Figure S4C) were generated out of iPSC-derived CMs. Assessment of BCT diameter did not reveal any difference between tissues generated of CMs from different clones (Figure S4D). However, the analysis of the functionality assessed by active forces of the BCTs demonstrated inter-clonal differences (Figures S4E and S4F). Overall, it seems that the m.13099G > A mutation in *ND5* with a heteroplasmy level of 38% in D#3 hUVEC C2-derived CMs resulted in a higher active force of BCTs compared with BCTs generated from the sister iPSC clone D#3 hUVEC C1.

DISCUSSION

Random genetic drift, positive selection, or clearance of mutated mtDNA, are suspected to shape the mutational landscape of mtDNA in iPSCs, but to which extent and at what stage those partly contradicting processes might act is widely unknown. In any case, occurrence of mtDNA mutations that alter the functionality of iPSC derivatives would exclude their clinical application.

Here, we have analyzed mtDNA variants in iPSCs and their corresponding parental cell populations during reprogramming, prolonged culture, and differentiation. We neither observed a distinct bottleneck nor any selection for or against mtDNA variants during reprogramming. Overall, the number of mtDNA molecules per iPSC was similar to the one in parental ECs. All mtDNA variants detected in iPSC clones have also been detected at different levels in the parental cells, although not in all cases with statistical confidence. Thus, we did not observe any evidence for substantial *de novo* mutagenesis, and inter-clonal differences in iPSCs apparently arose from the mitochondrial variant mosaicism within the parental cell population.

In contrast, during prolonged culture of iPSCs the heteroplasmy level of variants changed, while the mtDNA copy number per cell stayed uniform. Importantly, modeling the effect of random genetic drift on heteroplasmies revealed that a neutral model without selection cannot explain the observed changes. Interestingly, the selection acts pivotally against putatively actionable mutations, while neutral variants are accepted or even enriched. On a functional level, no difference between sister iPSC clones with and without *ND5* mutation at intermediate heteroplasmy level derived from the same parental cell population was observed. Although heterogeneity among single iPSCs or karyotypic abnormalities (Zambelli et al., 2018) might

have led to elimination of damaged cells or dominance of aberrant cell clones within the iPSC clone culture, this scenario is unlikely as simultaneously other variants (stable heteroplasmic group C variants) were maintained at a constant heteroplasmy level. It is more likely that even minor functional impact of mutations on mitochondria level led to selective mitophagy of damaged mitochondria and mtDNA via PINK1 and Parkin (PRKN) pathways, similarly as described for mtDNA integrity maintenance during germline transition (Kandul et al., 2016; Latorre-Pellicer et al., 2016; Lieber et al., 2019). In particular, *PRKN* was expressed at significantly higher levels in iPSCs compared with the somatic parental cells. Hence, the clearance of mtDNA mutations is presumably rather executed by an intrinsic process on the intracellular level than on an intercellular level.

The finding that the heteroplasmy levels of individual variants can increase by selection from the parental cell population or culture expansion highlights the need for careful consideration of variants with low heteroplasmy level. Although low heteroplasmy levels are generally regarded as not being clinically relevant, those levels could be augmented reaching the heteroplasmy threshold and impact functionality. Moreover, the heteroplasmy threshold at which a molecular phenotype manifests differs depending on variant and context (Sercel et al., 2021).

Importantly, our results demonstrate that, during targeted CM differentiation, the mtDNA copy number per cell is subjected to a distinct dynamic including an increase-reduction-increase cycle. Interestingly, this dynamic does not influence mtDNA average heteroplasmy levels. This observation leads to two conclusions: (1) the heteroplasmy level in iPSCs dictates the heteroplasmy level of the iPSC-derived CMs and (2) the observed dynamics of the mtDNA copy number during the course of the CM differentiation seems to be not yet strong enough to cause unequal mtDNA segregation.

While we did not observe any functional differences between sister iPSC clones with and without *ND5* mutation, CMs generated from D#3 hUVEC C2 with the m.13099G > A mutation at a heteroplasmy level of 38% resulted in BCTs exhibiting higher active forces than BCTs generated from the non-mutated sister clone. Although we cannot exclude further inter-clonal differences between both clones (Mannhardt et al., 2020), reduced levels of mitochondrial proteins (including ND5) can lead to reduction of ATP/ADP ratio, mitochondrial membrane potential, and mitochondrial Ca^{2+} uptake, followed by increment in cytosolic Ca^{2+}, activation of different signaling pathways, and altered cardiac functions, including hypertrophic cardiomyopathy-specific electrophysiological abnormalities, and elevated force (Bonora et al., 2019; Laude and Simpson, 2009; Li et al., 2018; Mannhardt et al., 2020). Therefore, depending on the (culture) conditions and maturation state, putatively actionable mtDNA variants, even at an intermediate heteroplasmy level, may eventually alter the functional characteristics of iPSC derivatives as reported previously (Hamalainen et al., 2013; Klein Gunnewiek et al., 2020; Wahlestedt et al., 2014; Yokota et al., 2015).

In conclusion, our results suggest that bottleneck effects in iPSC cultures might have been overestimated in the context of the mtDNA genetic pool. Our findings point toward a scenario in which intracellular positive and negative selection of mtDNA molecules mainly shapes the mutational landscape of the mitochondrial genome in iPSCs, while other mechanisms, such as random genetic drift and intercellular selection, exert minor impact.

EXPERIMENTAL PROCEDURES

Reprogramming and iPSC culture

Derivation and culture of ECs, virus production, retroviral reprogramming, iPSC characterization, and cultivation were performed as described previously (Haase et al., 2009) (supplemental experimental procedures). In total, 26 EC-derived iPSC clones were derived from 10 donors.

Total DNA extraction and determination of mitochondrial DNA copy number using quantitative real-time PCR

Total DNA was isolated using QIAamp DNA Blood mini kit (QIAGEN). Quantitative real-time PCR was performed on 25 ng total DNA per reaction in duplicates on Mastercycler ep realplex2 (Eppendorf) and with Absolute QPCR SYBR Green Mix (Thermo Scientific). The primer designing is described in the supplemental experimental procedures and primers are listed in Table S4. Sizes of amplicons and absence of nonspecific byproducts were confirmed via melting curve analysis using realplex software (Eppendorf). Quantification was obtained by both calculation of ddCt values and standard curve comparison. mtDNA copy number per cell was calculated as average mtDNA copy number relative to average gDNA copy number/2.

mtDNA extraction and mtDNA sequencing

The workflow for mtDNA sequencing and data processing is displayed in Figure S5A. mtDNA was extracted via QIAprep Spin Miniprep kit (QIAGEN) from early passage iPSC clones (mean p6.5), late passages (p30 and p50) of seven clones, and parental cell populations (mean p4.5). Entire mtDNA was amplified using two primer pairs (F2480A/R10858A [3:1] and F10653B/R2688B [1:1]) (Table S4) generating two overlapping PCR products (McElhoe et al., 2014). Two hundred nanograms of isolate were used as input, which equals ~5 × 10^8 mtDNA molecules of, on average, 5 × 10^6 iPSCs or 2.5 × 10^6 parental cells. Overall, mtDNA isolation via Miniprep kit and PCR amplification yielded, on average, a 12- and 15,000-fold increase of mtDNA over normal cellular content (Figure S5B). See also supplemental experimental procedures. Amplicons were purified by applying AMPure XP beads (Beckman

Coulter) in a 0.6× ratio, sheared by focused ultrasonication (Covaris), and quantified using a Qubit fluorimeter (Invitrogen). Sheared fragments were purified with AMPure XP beads (0.9× ratio), and 150 ng of each sample was fed to a library preparation using a NEBNext Ultra II DNA Library Preparation kit for Illumina (New England Biolabs) according to the manufacturer's instructions. Final concentration, fragment distribution (mean fragment length 600 bp), and quality were assessed on a Qubit fluorimeter and a Agilent Bioanalyzer. Libraries were sequenced as paired-end 250 bp reads using MiSeq Reagent Kit v.2 (Illumina).

Read alignment, variant calling and refinement

Post-run fastq files were imported into Galaxy (v.17.05) (Afgan et al., 2018) instance of RCU Genomics, Hannover Medical School, Germany, for read trimming, quality assessment, alignment, and variant calling. Quality and adapter trimming, as well as read mapping, are presented in the supplemental experimental procedures and as Galaxy workflow in Data S1. Reads were aligned to the human genome GRCh38 chromosome MT (the Cambridge Reference sequence rCRS [NC_012,920]). The coverage was 19,000 on average.

Variants were called utilizing FreeBayes (v.1.0.2; Galaxy implementation v.1.0.2.29-3) with filters set to ploidy 10, minimum coverage 100, and minimum AF (alternative frequency) 0.02. AF $\geq$ 0.02 as filter criterion was established by manually reviewing called variants within their read context (supplemental experimental procedures). A receiver operating characteristic curve with AF as discrimination threshold (Figure S5C) showed that AF 0.02 retrieves very high specificity while maintaining most true positive variants. False variants with AF $\geq$ 0.02 comprised the remaining adapter sequences and presumable sequencing errors of C-stretch or C-rich genomic regions and were manually removed. Comparison of dd0 samples of the CM differentiations of three iPSC clones (D#3C1, D#3C2, and D#37C10) and early iPSC passages (p6) of the respective clones proved that variants with AF $\geq$ 0.02 can be detected in sequencing replicates with repetitious accuracy. The dd0 samples represent independent replicates (separate sample preparation and sequencing) of the sequencing of the corresponding p6 iPSC clones. All heteroplasmic variants (AF 0.02–0.97) showed very similar AFs in both replicates (difference in AF: mean 0.01, median 0.01, range 0.00–0.03) (Table S5). Furthermore, we did not observe large variations in the heteroplasmy levels between dd0, dd5, and dd15 samples of the CM differentiation process of different iPSC clones (fold change ~1 independent of the variant heteroplasmy level), underlining the high accuracy of our approach (Table S5).

Detection of variants at very low AF

Furthermore, to investigate presence of a choice of variants at very low AF ($\leq$0.02) in iPSC clones or assess their pre-existence in parental cell populations, a total of 128 variants at 38 different genetic regions were examined individually within their genetic context as described previously (Kosanke et al., 2021) (supplemental experimental procedures). The mean error rate and detection limit were calculated individually for every variant, and the presence of variant was confirmed with p = 0.05 against background of errors (Figure S5D; Table S2). Overall, the average coverage of the variant regions was 22,000 and detection limit was 1 read in ~340 (SD 450), which equals, on average, a detection sensitivity down to AF 0.003.

Variant annotation and prediction of functional consequences

Variant annotation was performed using the web interface of the Ensembl Variant effect predictor (VEP) (v.95) (assembly GRCh38.p12) (McLaren et al., 2016). Haplogroups and corresponding haplotype variants were identified using the HaploGrep algorithm (Weissensteiner et al., 2016). MITOMAP (a human mitochondrial genome database, r103) was utilized to retrieve population frequencies (NCBI GenBank frequency [GB]) of variants. Variants with GB frequency $\geq$ 0.02 were considered to be polymorphic.

Prediction of functional consequences was obtained from Ensembl VEP and HmtVar (Preste et al., 2019). The functional consequence of a variant was classified by a consensus based on the *in silico* predictions of snpEff impact prediction, Condel (consensus of SIFT and Polyphen2), CADD, and HmtVar, which comprises predictions of MutPred, Panther, PhD SNP, Polyphen2, and SNPs&GO, and contains information about variants in protein and RNA coding regions. If a variant had a harmful designation by snpEff (high impact = frameshift) or at least by two of the other algorithms (Condel = deleterious, CADD phred > 12, HmtVar = pathogenic), it was considered as putatively actionable.

Modeling heteroplasmy variance over time

A model by Aryaman et al. (2019) was adapted for modeling heteroplasmy variance over time.

$$V(h) \approx fs \frac{2\mu t}{n}[h(1-h)],$$

where *fs* is a factor for fragmentation, which indicates the ratio of fused mitochondria, μ is a factor for mitophagy rate, and h is the heteroplasmy level. As iPSCs are featured by unfused mitochondria, *fs* was excluded in our modeling. n represents the mtDNA copy number/cell. Determination of the mtDNA copy number in iPSCs (n) in p6, p30, and p50 showed that n stayed constant over time in culture and was, on average, 1,000. Heteroplasmy variance ($V(h)$) was calculated for different heteroplasmy levels with different μ values to assess effect of genetic drift (without selection, μ = 1) and selection (μ = 2, 5, 10, and 50).

Karyotype analysis

Preparation of metaphases, fluorescence R-banding, and analysis of at least 10 metaphases were performed according to standard procedures (supplemental experimental procedures).

Differentiation of CM, and BCT generation and analysis

For embryoid body formation (dd −3), 1 × 10^6 iPSCs/well were aggregated in 3 mL E8 medium containing 10 μM Rho-Kinase inhibitor Y-27632 (RI) on low attachment six-well plates (Greiner Bio-one) and an orbital shaker (70 rpm; Infors). CM differentiation, and BCT generation and analysis, were performed as described earlier (Halloin et al., 2019; Kensah et al., 2011, 2013) (supplemental experimental procedures).

Live-cell staining and flow cytometric analysis

Live-cell staining was performed of adherent cells with MitoTracker, ROS Brite 670, and TMRM (25 nM; Thermo Fisher Scientific) diluted in Hank's solution (Gibco) with 20 mM HEPES (Sigma-Aldrich) (HHBS) according to the manufacturer's recommendation for 45 min. A list of antibodies and dyes is provided in Table S6. Cells were dissociated by Versene (Gibco) or trypsin/EDTA treatment for iPSCs or ECs, respectively, resuspended in HHBS buffer, filtered, and analyzed by flow cytometry. Flow cytometry was executed on a MACSQuant analyzer (Miltenyi Biotec) and data were analyzed with FlowJo (v.10).

Immunofluorescence staining and microscopic analysis

ECs, iPSCs, and CMs were seeded on cover slides and, after a culture period of 1–2 days for ECs and iPSCs, and 3 days for CMs, cells were fixed, permeabilized, and stained with anti-ATPIF1 antibody (Table S6) (supplemental experimental procedures). Cells were analyzed using an Axioserver A1 fluorescent microscope (Zeiss) and Axiovision (v.4.71) software.

Measurement of glucose consumption and lactate production rate

iPSCs were cultured as monolayers in house-made E8 medium. On day 1 after cell seeding, the medium was exchanged and, on the subsequent 2 days, lactate and glucose concentrations from cell-free supernatant were measured employing Biosen C-Line glucose and lactate analyzer (EKF Diagnostics). On each day of analysis, the cell numbers were counted using a Neubauer chamber. Technical triplicates initiated from the same starting cell population were analyzed for each sample and time point. Yield coefficient of lactate from glucose was calculated as described previously (Kropp et al., 2016).

Gene expression analysis via quantitative real-time PCR

Total RNA was isolated via RNeasy Kit (Macherey-Nagel, Düren, Germany) and reverse transcribed utilizing Superscript II (Life Technologies) and random primers according to the manufacturer's instructions. Quantitative real-time PCR was performed on 5 ng cDNA per reaction in duplicates on a CFX Connecet Real-time system (Bio-Rad) and with Absolute QPCR SYBR Green Mix (Thermo Scientific). Primers are listed in Table S4. Absence of nonspecific byproducts was confirmed via melting curve analysis. Expression levels of target genes were normalized to *GAPDH* and *RPL13*A transcript levels. The analysis was performed using Bio-Rad CFX Maestro 1.1 (v.4.1.2433.1219) software.

Statistical analyses

If not stated otherwise, N refers to independent batches of cells. GraphPad Prism (v.6.07), RStudio (v.1.1.463; R v.3.5.1), or Bio-Rad CFX Maestro 1.1 software were employed for statistical analysis and visualization. Results are presented as mean and SD. The D'Agostino-Pearson omnibus normality test was executed to check if samples were normally distributed. In cases where the sample size was not sufficiently large, the Shapiro-Wilk normality test and Kolmogorov-Smirnov test were applied. Unpaired two-tailed t test and non-parametric two-tailed Mann Whitney test were employed as appropriate to test for significant differences between groups. One-way ANOVA with post hoc Tukey's multiple comparisons test and Kruskal-Wallis test with post hoc Dunn multiple comparison test, respectively, were used to test for significant differences between multiple groups.

Comparison of metabolic features of mutated against wild-type iPSC clones or of CMs derived thereof, was underlined by non-parametric Wilcoxon signed-rank test for derivation from hypothetical value of 1.

Local error rates of the amplicon sequencing was calculated and (pre-)existence of variants assessed ($p < 0.05$) as described previously (Kosanke et al., 2021) (supplemental experimental procedures).

Code availability

Sequencing data analysis was mainly performed on the Galaxy (v.17.05) (Afgan et al., 2018) instance of the RCU Genomics, Hannover Medical School, Germany. The workflow is available in Data S1.

Data availability

Data are deposited in the European Genome-phenome Archive at the European Bioinformatics Institute. The accession number for the study reported in this paper is EGA: EGAS00001005560.

SUPPLEMENTAL INFORMATION

Supplemental information can be found online at https://doi.org/10.1016/j.stemcr.2021.08.016.

AUTHOR CONTRIBUTIONS

M.K. contributed to designing and coordinating the study, performed, experiments, collected and analyzed data, and wrote the manuscript. C.D. and L.W. performed sequencing and contributed to analyzing bioinformatics data. T.K. performed the experiments. M.D. provided technical assistance in fragment library construction and sequencing. J.G., K.M., and M. Sievert provided technical assistance in performing experiments. M. Szepes, I.G., and A.M. coordinated and performed cardiomyocyte differentiation and analysis. G.G. provided karyotype analysis. U.M. designed and coordinated the study.

CONFLICTS OF INTEREST

The authors declare no competing interests.

ACKNOWLEDGMENTS

Many thanks to K. Osetek for isolation of hUVEC and hSVEC, and their reprogramming into iPSCs, to P. Stiefel for several HSVEC isolations, and to T. Scheper for providing bFGF. We are also thankful to S. Rojas, T. Goecke, and other surgical colleagues, who provided human tissue samples. We thank J. Thomson for providing the reprogramming plasmids via Addgene and D. Trono for providing the lentiviral packaging and transfer plasmids psPAX2 and pMD2.G. Many thanks as well to A. Haase and S. Merkert for a

critical reading of the manuscript. This work was funded by the German Federal Ministry of Education and Research (CARPuD, 01GM1110A-C; iCARE 01EK1601A), the German Center for Lung Research (DZL, 82DZL00201, 82DZL00401) the German Research Foundation (Cluster of Excellence REBIRTH, EXC 62/3), the Ministry for Science and Culture Lower Saxony (Niedersächsisches Vorab, REBIRTH, ZN 3440), and by the Sächsische Aufbau-Bank/Vita34.

Received: November 12, 2020
Revised: August 26, 2021
Accepted: August 27, 2021
Published: September 23, 2021

REFERENCES

Afgan, E., Baker, D., Batut, B., van den Beek, M., Bouvier, D., Cech, M., Chilton, J., Clements, D., Coraor, N., Gruning, B.A., et al. (2018). The Galaxy platform for accessible, reproducible and collaborative biomedical analyses: 2018 update. Nucleic Acids Res. *46*, W537–W544.

Andrews, P.W., Ben-David, U., Benvenisty, N., Coffey, P., Eggan, K., Knowles, B.B., Nagy, A., Pera, M., Reubinoff, B., Rugg-Gunn, P.J., et al. (2017). Assessing the safety of human pluripotent stem cells and their derivatives for clinical applications. Stem Cell Reports *9*, 1–4.

Aryaman, J., Bowles, C., Jones, N.S., and Johnston, I.G. (2019). Mitochondrial network state scales mtDNA genetic dynamics. Genetics *212*, 1429–1443.

Bonora, M., Wieckowski, M.R., Sinclair, D.A., Kroemer, G., Pinton, P., and Galluzzi, L. (2019). Targeting mitochondria for cardiovascular disorders: therapeutic potential and obstacles. Nat. Rev. Cardiol. *16*, 33–55.

Cao, L., Shitara, H., Sugimoto, M., Hayashi, J., Abe, K., and Yonekawa, H. (2009). New evidence confirms that the mitochondrial bottleneck is generated without reduction of mitochondrial DNA content in early primordial germ cells of mice. PLoS Genet. *5*, e1000756.

Cherry, A.B., Gagne, K.E., McLoughlin, E.M., Baccei, A., Gorman, B., Hartung, O., Miller, J.D., Zhang, J., Zon, R.L., Ince, T.A., et al. (2013). Induced pluripotent stem cells with a mitochondrial DNA deletion. Stem Cells *31*, 1287–1297.

Chinnery, P.F., and Prudent, J. (2019). De-fusing mitochondria defuses the mtDNA time-bomb. Cell Res. *29*, 781–782.

Clayton, D.A. (1991). Replication and transcription of vertebrate mitochondrial DNA. Annu. Rev. Cell Biol. *7*, 453–478.

Copeland, W.C., Wachsman, J.T., Johnson, F.M., and Penta, J.S. (2002). Mitochondrial DNA alterations in cancer. Cancer Invest. *20*, 557–569.

Deuse, T., Hu, X., Agbor-Enoh, S., Koch, M., Spitzer, M.H., Gravina, A., Alawi, M., Marishta, A., Peters, B., Kosaloglu-Yalcin, Z., et al. (2019). De novo mutations in mitochondrial DNA of iPSCs produce immunogenic neoepitopes in mice and humans. Nat. Biotechnol. *37*, 1137–1144.

Floros, V.I., Pyle, A., Dietmann, S., Wei, W., Tang, W.C.W., Irie, N., Payne, B., Capalbo, A., Noli, L., Coxhead, J., et al. (2018). Segregation of mitochondrial DNA heteroplasmy through a developmental genetic bottleneck in human embryos. Nat. Cell Biol. *20*, 144–151.

Folmes, C.D., Martinez-Fernandez, A., Perales-Clemente, E., Li, X., McDonald, A., Oglesbee, D., Hrstka, S.C., Perez-Terzic, C., Terzic, A., and Nelson, T.J. (2013). Disease-causing mitochondrial heteroplasmy segregated within induced pluripotent stem cell clones derived from a patient with MELAS. Stem Cells *31*, 1298–1308.

Haase, A., Olmer, R., Schwanke, K., Wunderlich, S., Merkert, S., Hess, C., Zweigerdt, R., Gruh, I., Meyer, J., Wagner, S., et al. (2009). Generation of induced pluripotent stem cells from human cord blood. Cell Stem Cell *5*, 434–441.

Halloin, C., Schwanke, K., Lobel, W., Franke, A., Szepes, M., Biswanath, S., Wunderlich, S., Merkert, S., Weber, N., Osten, F., et al. (2019). Continuous WNT control enables advanced hPSC cardiac processing and prognostic surface marker identification in chemically defined suspension culture. Stem Cell Reports *13*, 366–379.

Hamalainen, R.H., Manninen, T., Koivumaki, H., Kislin, M., Otonkoski, T., and Suomalainen, A. (2013). Tissue- and cell-type-specific manifestations of heteroplasmic mtDNA 3243A>G mutation in human induced pluripotent stem cell-derived disease model. Proc. Natl. Acad. Sci. *110*, E3622–E3630.

Hung, S.S., Van Bergen, N.J., Jackson, S., Liang, H., Mackey, D.A., Hernandez, D., Lim, S.Y., Hewitt, A.W., Trounce, I., Pebay, A., et al. (2016). Study of mitochondrial respiratory defects on reprogramming to human induced pluripotent stem cells. Aging (Albany NY) *8*, 945–957.

Kandul, N.P., Zhang, T., Hay, B.A., and Guo, M. (2016). Selective removal of deletion-bearing mitochondrial DNA in heteroplasmic *Drosophila*. Nat. Commun. *7*, 13100.

Kang, E., Wang, X., Tippner-Hedges, R., Ma, H., Folmes, C.D., Gutierrez, N.M., Lee, Y., Van Dyken, C., Ahmed, R., Li, Y., et al. (2016). Age-related accumulation of somatic mitochondrial DNA mutations in adult-derived human iPSCs. Cell Stem Cell *18*, 625–636.

Kensah, G., Gruh, I., Viering, J., Schumann, H., Dahlmann, J., Meyer, H., Skvorc, D., Bar, A., Akhyari, P., Heisterkamp, A., et al. (2011). A novel miniaturized multimodal bioreactor for continuous in situ assessment of bioartificial cardiac tissue during stimulation and maturation. Tissue Eng. Part C Methods *17*, 463–473.

Kensah, G., Roa Lara, A., Dahlmann, J., Zweigerdt, R., Schwanke, K., Hegermann, J., Skvorc, D., Gawol, A., Azizian, A., Wagner, S., et al. (2013). Murine and human pluripotent stem cell-derived cardiac bodies form contractile myocardial tissue in vitro. Eur. Heart J. *34*, 1134–1146.

Klein Gunnewiek, T.M., Van Hugte, E.J.H., Frega, M., Guardia, G.S., Foreman, K., Panneman, D., Mossink, B., Linda, K., Keller, J.M., Schubert, D., et al. (2020). m.3243A > G-induced mitochondrial dysfunction impairs human neuronal development and reduces neuronal network activity and synchronicity. Cell Rep. *31*, 107538.

Kosanke, M., Osetek, K., Haase, A., Wiehlmann, L., Davenport, C., Schwarzer, A., Adams, F., Schambach, A., Merkert, S., Wunderlich, S., et al. (2021). Reprogramming enriches for somatic cell clones with small scale mutations in cancer-associated genes. Mol. Ther. *S1525-0016*, 00194–00195.

Kropp, C., Kempf, H., Halloin, C., Robles-Diaz, D., Franke, A., Scheper, T., Kinast, K., Knorpp, T., Joos, T.O., Haverich, A., et al. (2016). Impact of feeding strategies on the scalable expansion of human pluripotent stem cells in single-use stirred tank bioreactors. Stem Cells Transl. Med. *5*, 1289–1301.

Latorre-Pellicer, A., Moreno-Loshuertos, R., Lechuga-Vieco, A.V., Sánchez-Cabo, F., Torroja, C., Acín-Pérez, R., Calvo, E., Aix, E., González-Guerra, A., Logan, A., et al. (2016). Mitochondrial and nuclear DNA matching shapes metabolism and healthy ageing. Nature *535*, 561–565.

Laude, A.J., and Simpson, A.W. (2009). Compartmentalized signalling: Ca^{2+} compartments, microdomains and the many facets of Ca2+ signalling. FEBS J. *276*, 1800–1816.

Li, S., Pan, H., Tan, C., Sun, Y., Song, Y., Zhang, X., Yang, W., Wang, X., Li, D., Dai, Y., et al. (2018). Mitochondrial dysfunctions contribute to hypertrophic cardiomyopathy in patient iPSC-derived cardiomyocytes with MT-RNR2 mutation. Stem Cell Reports *10*, 808–821.

Lieber, T., Jeedigunta, S.P., Palozzi, J.M., Lehmann, R., and Hurd, T.R. (2019). Mitochondrial fragmentation drives selective removal of deleterious mtDNA in the germline. Nature *570*, 380–384.

Ma, T., Li, J., Xu, Y., Yu, C., Xu, T., Wang, H., Liu, K., Cao, N., Nie, B.M., Zhu, S.Y., et al. (2015). Atg5-independent autophagy regulates mitochondrial clearance and is essential for iPSC reprogramming. Nat. Cell Biol. *17*, 1379–1387.

Maitra, A., Arking, D.E., Shivapurkar, N., Ikeda, M., Stastny, V., Kassauei, K., Sui, G., Cutler, D.J., Liu, Y., Brimble, S.N., et al. (2005). Genomic alterations in cultured human embryonic stem cells. Nat. Genet. *37*, 1099–1103.

Mannhardt, I., Saleem, U., Mosqueira, D., Loos, M.F., Ulmer, B.M., Lemoine, M.D., Larsson, C., Ameen, C., de Korte, T., Vlaming, M.L.H., et al. (2020). Comparison of 10 control hPSC lines for drug screening in an engineered heart tissue format. Stem Cell Reports *15*, 983–998.

McElhoe, J.A., Holland, M.M., Makova, K.D., Su, M.S., Paul, I.M., Baker, C.H., Faith, S.A., and Young, B. (2014). Development and assessment of an optimized next-generation DNA sequencing approach for the mtgenome using the Illumina MiSeq. Forensic Sci. Int. Genet. *13*, 20–29.

McLaren, W., Gil, L., Hunt, S.E., Riat, H.S., Ritchie, G.R., Thormann, A., Flicek, P., and Cunningham, F. (2016). The Ensembl variant effect predictor. Genome Biol. *17*, 122.

Naue, J., Horer, S., Sanger, T., Strobl, C., Hatzer-Grubwieser, P., Parson, W., and Lutz-Bonengel, S. (2015). Evidence for frequent and tissue-specific sequence heteroplasmy in human mitochondrial DNA. Mitochondrion *20*, 82–94.

Park, C.B., and Larsson, N.G. (2011). Mitochondrial DNA mutations in disease and aging. J. Cell Biol. *193*, 809–818.

Payne, B.A., Wilson, I.J., Yu-Wai-Man, P., Coxhead, J., Deehan, D., Horvath, R., Taylor, R.W., Samuels, D.C., Santibanez-Koref, M., and Chinnery, P.F. (2013). Universal heteroplasmy of human mitochondrial DNA. Hum. Mol. Genet. *22*, 384–390.

Perales-Clemente, E., Cook, A.N., Evans, J.M., Roellinger, S., Secreto, F., Emmanuele, V., Oglesbee, D., Mootha, V.K., Hirano, M., Schon, E.A., et al. (2016). Natural underlying mtDNA heteroplasmy as a potential source of intra-person hiPSC variability. EMBO J. *35*, 1979–1990.

Preste, R., Vitale, O., Clima, R., Gasparre, G., and Attimonelli, M. (2019). HmtVar: a new resource for human mitochondrial variations and pathogenicity data. Nucleic Acids Res. *47*, D1202–D1210.

Prigione, A., Fauler, B., Lurz, R., Lehrach, H., and Adjaye, J. (2010). The senescence-related mitochondrial/oxidative stress pathway is repressed in human induced pluripotent stem cells. Stem Cells *28*, 721–733.

Prigione, A., Hossini, A.M., Lichtner, B., Serin, A., Fauler, B., Megges, M., Lurz, R., Lehrach, H., Makrantonaki, E., Zouboulis, C.C., et al. (2011). Mitochondrial-associated cell death mechanisms are reset to an embryonic-like state in aged donor-derived iPS cells harboring chromosomal aberrations. PLoS One *6*, e27352.

Roze, D., Rousset, F., and Michalakis, Y. (2005). Germline bottlenecks, biparental inheritance and selection on mitochondrial variants: a two-level selection model. Genetics *170*, 1385–1399.

Sercel, A.J., Carlson, N.M., Patananan, A.N., and Teitell, M.A. (2021). Mitochondrial DNA dynamics in reprogramming to pluripotency. Trends Cell Biol. *31*, 311–323.

Shakiba, N., Fahmy, A., Jayakumaran, G., McGibbon, S., David, L., Trcka, D., Elbaz, J., Puri, M.C., Nagy, A., van der Kooy, D., et al. (2019). Cell competition during reprogramming gives rise to dominant clones. Science *364*, eaan0925.

Wahlestedt, M., Ameur, A., Moraghebi, R., Norddahl, G.L., Sten, G., Woods, N.B., and Bryder, D. (2014). Somatic cells with a heavy mitochondrial DNA mutational load render induced pluripotent stem cells with distinct differentiation defects. Stem Cells *32*, 1173–1182.

Wei, W., Tuna, S., Keogh, M.J., Smith, K.R., Aitman, T.J., Beales, P.L., Bennett, D.L., Gale, D.P., Bitner-Glindzicz, M.A.K., Black, G.C., et al. (2019). Germline selection shapes human mitochondrial DNA diversity. Science *364*, eaau6520.

Weissbein, U., Benvenisty, N., and Ben-David, U. (2014). Quality control: genome maintenance in pluripotent stem cells. J. Cell Biol. *204*, 153–163.

Weissensteiner, H., Pacher, D., Kloss-Brandstatter, A., Forer, L., Specht, G., Bandelt, H.J., Kronenberg, F., Salas, A., and Schonherr, S. (2016). HaploGrep 2: mitochondrial haplogroup classification in the era of high-throughput sequencing. Nucleic Acids Res. *44*, W58–W63.

Yokota, M., Hatakeyama, H., Okabe, S., Ono, Y., and Goto, Y. (2015). Mitochondrial respiratory dysfunction caused by a heteroplasmic mitochondrial DNA mutation blocks cellular reprogramming. Hum. Mol. Genet. *24*, 4698–4709.

Yoshihara, M., Araki, R., Kasama, Y., Sunayama, M., Abe, M., Nishida, K., Kawaji, H., Hayashizaki, Y., and Murakawa, Y. (2017). Hotspots of de novo point mutations in induced pluripotent stem cells. Cell Rep. *21*, 308–315.

Zambelli, F., Mertens, J., Dziedzicka, D., Sterckx, J., Markouli, C., Keller, A., Tropel, P., Jung, L., Viville, S., Van de Velde, H., et al. (2018). Random mutagenesis, clonal events, and embryonic or somatic origin determine the mtDNA variant type and load in human pluripotent stem cells. Stem Cell Reports. *11*, 102–114.

Stem Cell Reports, Volume *16*

Supplemental Information

iPSC culture expansion selects against putatively actionable mutations in the mitochondrial genome

Maike Kosanke, Colin Davenport, Monika Szepes, Lutz Wiehlmann, Tim Kohrn, Marie Dorda, Jonas Gruber, Kaja Menge, Maike Sievert, Anna Melchert, Ina Gruh, Gudrun Göhring, and Ulrich Martin

Supplemental Information:

Supplemental Figures and Tables:

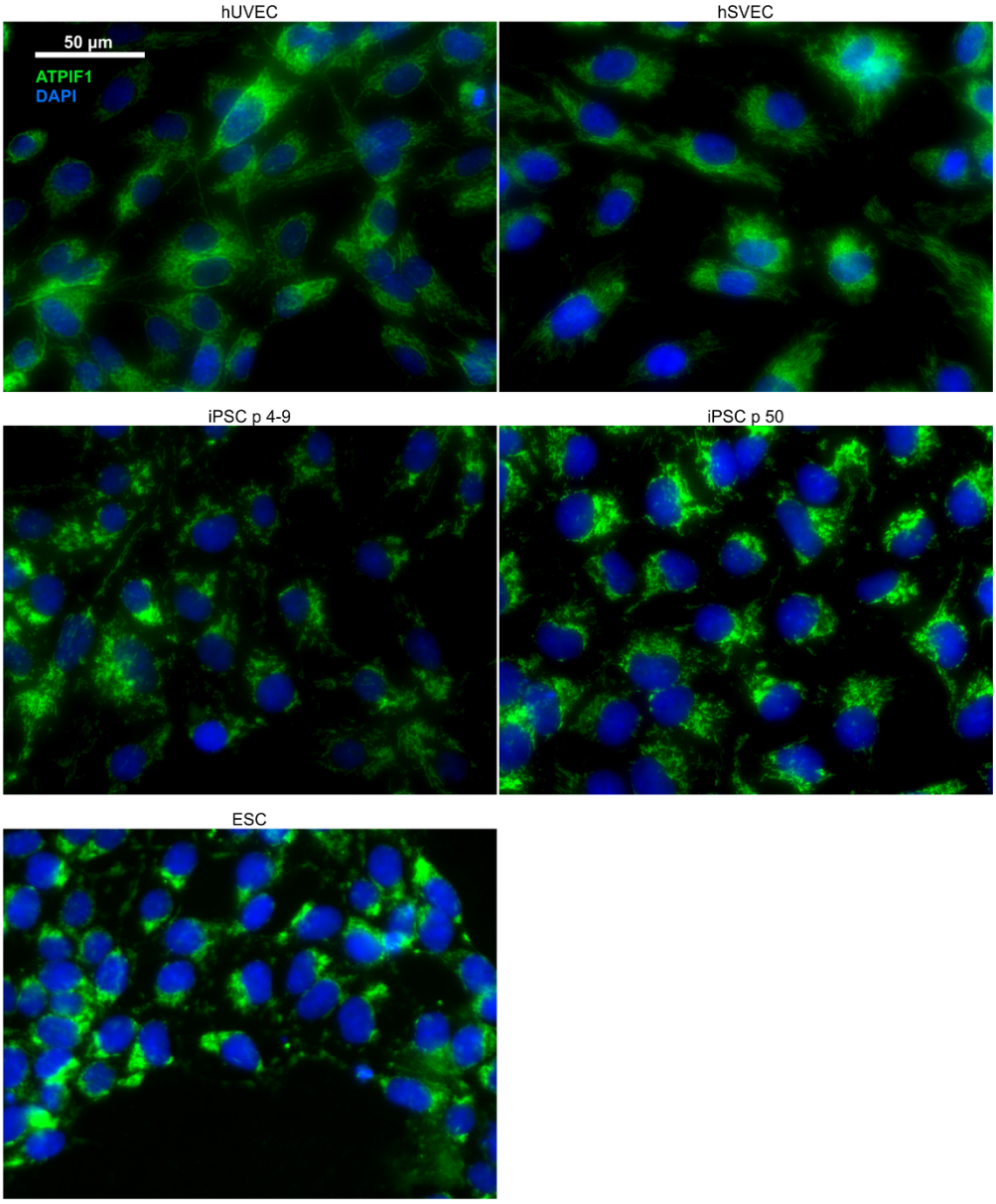

Figure S1: Mitochondrial network in ECs, iPSCs, and ESCs; Mentioned in first and second Result section. Adherent ECs (umbilical vein (hUVEC) and saphenous vein (hSVEC)), iPSCs of early and late passage, and ESCs were seeded on gelatine or Geltrex coated glass cover slides, cultured for 2-3 days in EMG2 or E8 medium, fixed with PFA, stained with anti-ATPIF1 (ATP synthase subunit IF1) antibody and DAPI nuclear staining, and analyzed by fluorescence microscopy. Pictures of different representative donors and clones are shown. Mitochondria are displayed in green and nuclei staining in blue. Scale bar 50µm.

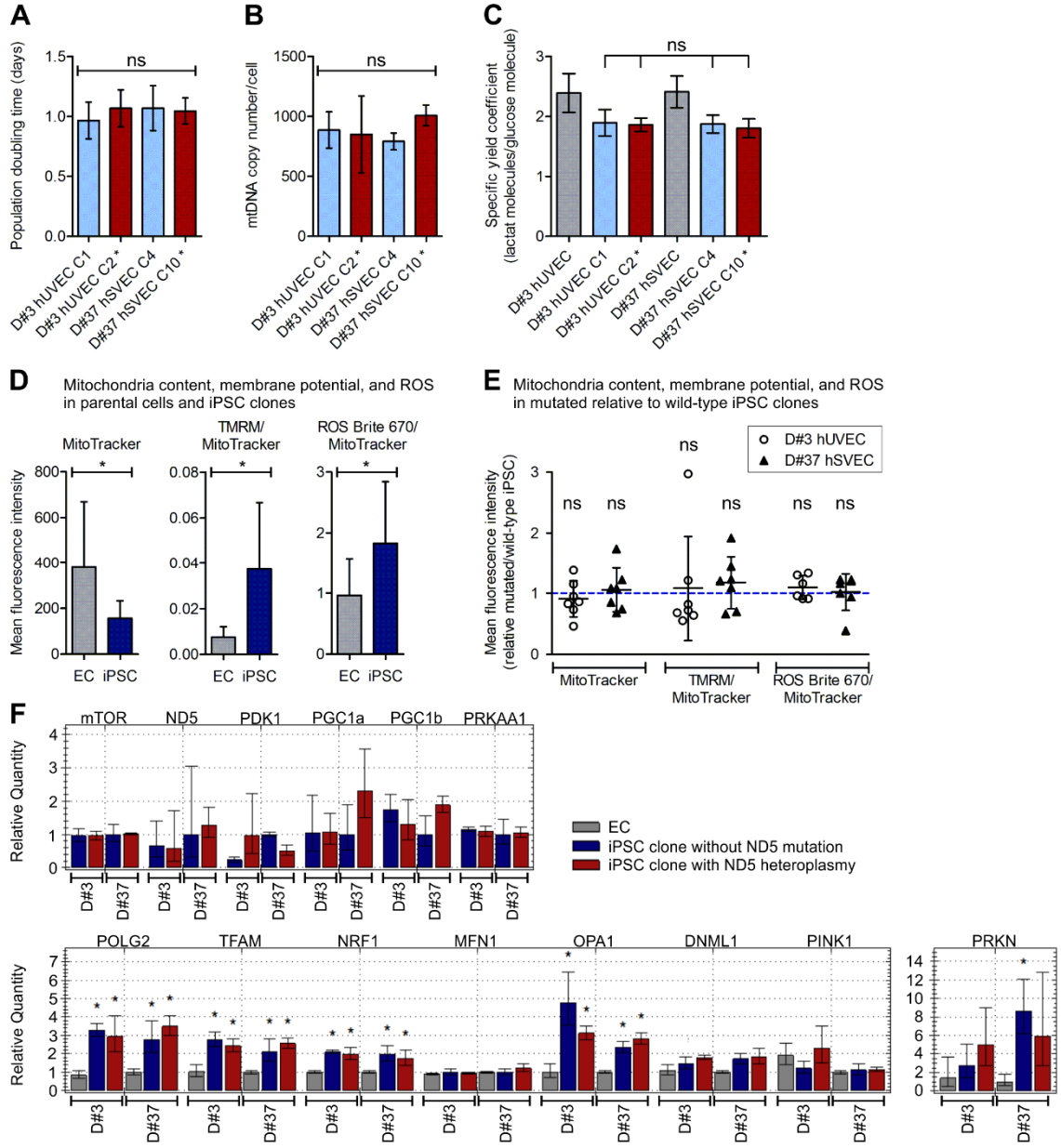

Figure S2: No detectable effect of specific *ND5* mutations on the functionality of undifferentiated iPSCs; Addressed in first Result section. iPSC clones with putatively actionable *ND5* mutations at an intermediate heteroplasmy level (D#37 hSVEC C10 with m.12686T>C at heteroplasmy level of ~23% and D#3 hUVEC C2 with m.13099G>A and ~38% heteroplasmy) and their sister iPSC clones without *ND5* mutations derived from the same parental cell population were analyzed. Mutated iPSC clones are marked with *. **A** Population doubling calculated as time in days needed for doubling of cell number measured by cell counting. Cell numbers were determined over 8-12 passages. N = 8-12 independent cell harvests each with 3 technical replicates. Mean with SD. Tested for significant differences by One-way Anova with Tukey's Multiple Comparison Test. **B** mtDNA copy number per iPSCs. Mean with SD. N = 2-4. No significant differences (One-way Anova). **C** Yield coefficient of lactate from glucose. Mean with SD. EC N = 2-3 and iPSC N = 3-4 biological replicates each with 2-3 technical replicates. Statistical analysis perfumed using One-way Anova. **D-E** Determination of mitochondrial content (MitoTracker), membrane potential (TMRM), and reactive oxygen species (ROS Brite 670) per cell via live cell staining and flow cytometric analysis. **D** Quantification calculated as geometric mean of fluorescence intensity of staining-positive populations. Mean with SD. EC N = 4; iPSC N = 8 including 4 independent batches of cells of mutated and 4 of wild-type clones. * indicates significant difference between groups (p-value < 0.05; Unpaired two-tailed t-test or nonparametric two-tailed Mann Whitney test). **E** Comparison of metabolic features of mutated against wild-type iPSC clones. Plot displays the deviation of values measured in mutated iPSC clones from the values in their wild-type counterparts quantified by geometric mean of fluorescence intensity and normalized to mitochondrial content (MitoTracker geometric mean). Mean

with SD. N = 7. Statistical analysis: Wilcoxon signed-rank test for derivation from hypothetical value of 1. **F** Gene expression analysis in iPSC clones and parental cells for genes involved in metabolism ((*mTOR*, *ND5*, *PDK1*, *PGC1a*, *PGC1b*, *PRKAA1*), mtDNA replication and transcription (*POLG2*, *TFAM*, *NRF1*), mitochondria dynamics (*MFN1*, *OPA1*, *DNML1*), and mitophagy (*PINK1*, *PRKN*) using qRT-PCR. Expression of all genes were normalized against housekeeping gene expression and is displayed relative to control iPSC clone D#37 hSVEC C4 (upper graph) or parental cells (D#37 hSVEC EC) (lower graph). Mean with SD; N = 3. Statistical analysis: One-way Anova with Tukey's Multiple Comparison Test for significant differences of gene expression in iPSC clones compared to parental cells (p-value < 0.05). No significant differences in gene expression between iPSC clones (One-way Anova with Tukey's Multiple Comparison).

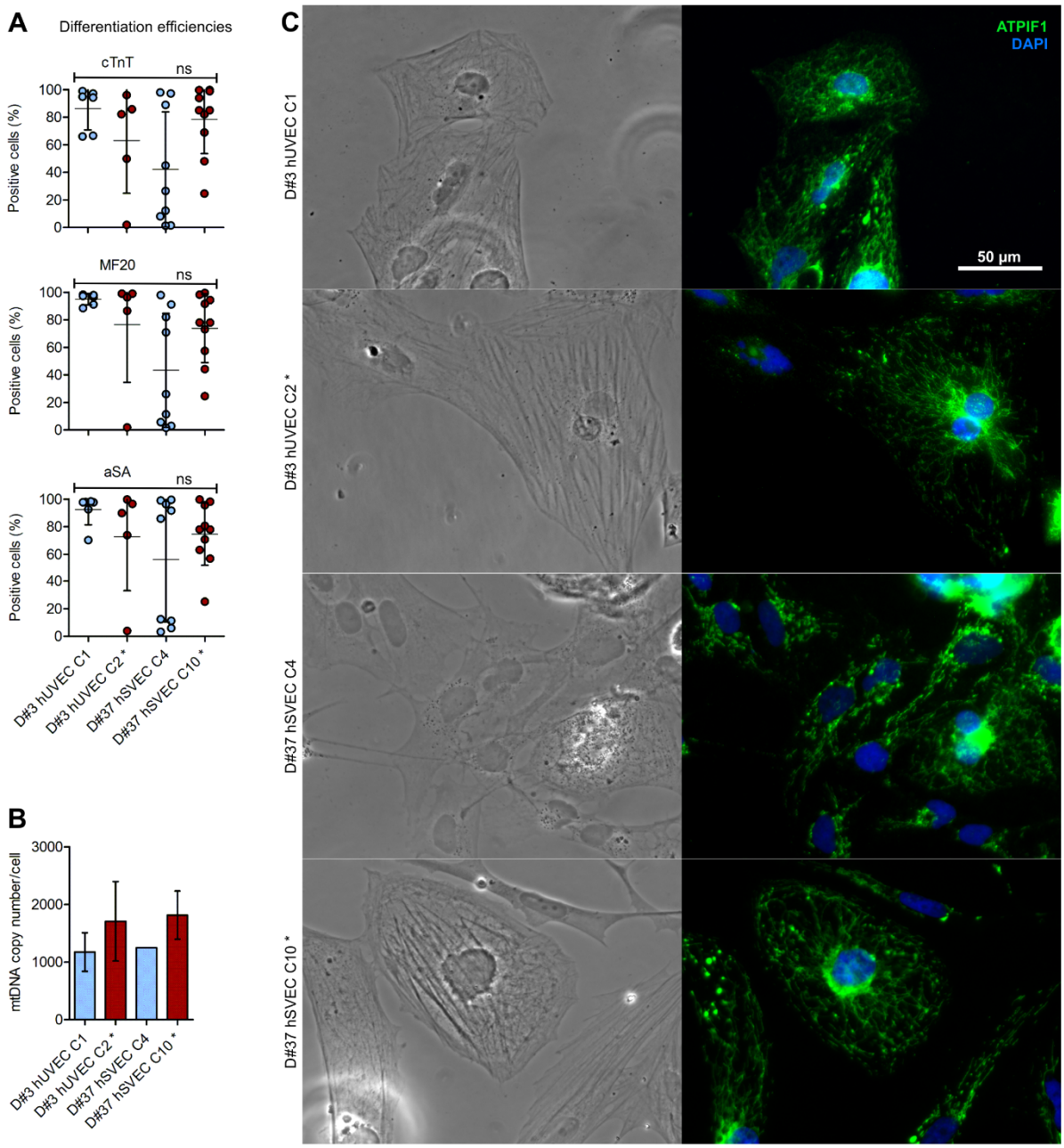

Figure S3: Intermediate heteroplasmy level of putatively actionable *ND5* mutation does not alter differentiation potential of iPSCs into CMs; Mentioned in third Result section. 2 mutated iPSC clones (marked with *; D#3 hUVEC C2 and D#37 hSVEC C10) each harbor a different putatively actionable mutation in *ND5* at intermediate heteroplasmy level and their isogenic sister iPSC clones were differentiated into CMs. **A** Differentiation efficiency quantified by positive staining for cTnT (Troponin-T), MF20 (MYH1E), and aSA (Sarcomeric α-actinin) and flow cytometry analysis at differentiation day (dd) 14. Mean with SD. N = 5-10 independent differentiations. Statistical analysis: Kruskal-Wallis test with Dunn's Multiple Comparison Test. **B** mtDNA copy number per CM determined at dd12-20. Mean with SD. N = 1 or 3 differentiations with differentiation efficiencies > 80% CM-marker positive cells. **C** CM at dd15 were seeded on fibronectin/gelatin (50µg/ml in 0.02% gelatin) coated glass cover slides, cultured for 3 days in differentiation medium, fixed with PFA, stained with anti-ATPIF1 (ATP synthase subunit IF1) antibody (green) and DAPI nuclear staining (blue), and analyzed by fluorescence microscopy. Scale bar 50µm.

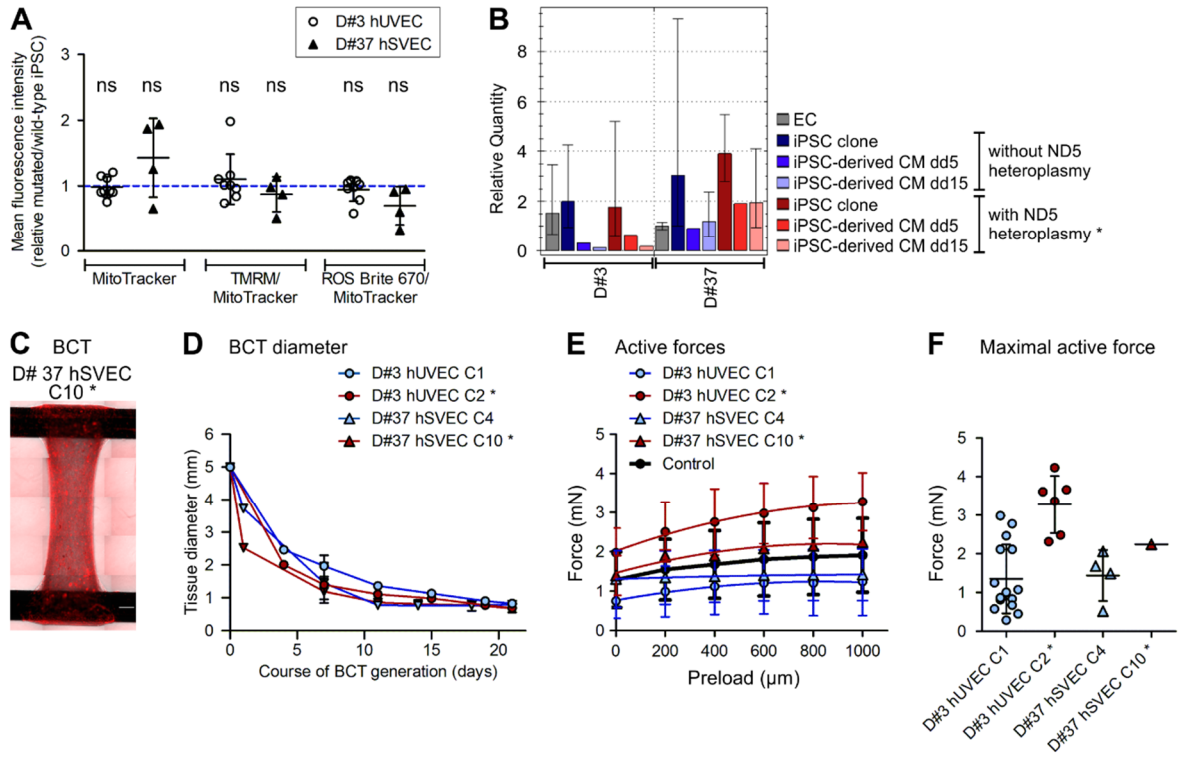

Figure S4: Impact of specific *ND5* mutations on CM functionality; Addressed in third Result section. iPSC clones with putatively actionable *ND5* mutations at an intermediate heteroplasmy level (marked with *; D#37 hSVEC C10 with m.12686T>C at heteroplasmy level of ~23% and D#3 hUVEC C2 with m.13099G>A and ~38% heteroplasmy) and their sister iPSC clones derived from the same parental cell population were differentiated into CMs. **A** Determination of mitochondrial content (MitoTracker), membrane potential (TMRM), and reactive oxygen species (ROS Brite 670) per cell via live cell staining and flow cytometric analysis. Comparison of metabolic features of mutated against wild-type iPSC-derived CMs. Plot displays the deviation of values measured in CMs derived of mutated iPSC clones from the values in their wild-type counterparts quantified by geometric mean of fluorescence intensity and normalized to mitochondrial content (MitoTracker geometric mean). Mean with SD. N = 4-8. Values do not deviate significantly from hypothetical value of 1 (Wilcoxon signed-rank test). **B** Relative quantification of *ND5* expression in parental endothelial cells (EC), iPSC clones and iPSC-derive CMs at differentiation day (dd) 5 and 15 using qRT-PCR. For each sample expression of *ND5* was normalized against housekeeping gene expression and is displayed relative to D#37 hSVEC EC. Mean with SD; iPSC N = 3; CM N = 1-2. **C-F** Bioartificial cardiac tissue (BCTs) were generated and active forces were measured. **C** Representative pictures of one BCT. Scale bar 500µm. **D** Diameter of BCT measured over course of BCT generation. Mean ± SD; N = 5-7 BCTs; 1-2 differentiations (biological replicates). **E** Active forces. Mean ± SD; N = 1-15 BCTs; 1-2 differentiations. Control N = 44 BCTs from 9 independent differentiations of 3 standard clonal iPSC lines. **F** Maximum active force. Mean ± SD; N = 1-15 BCTs; 1-2 differentiations.

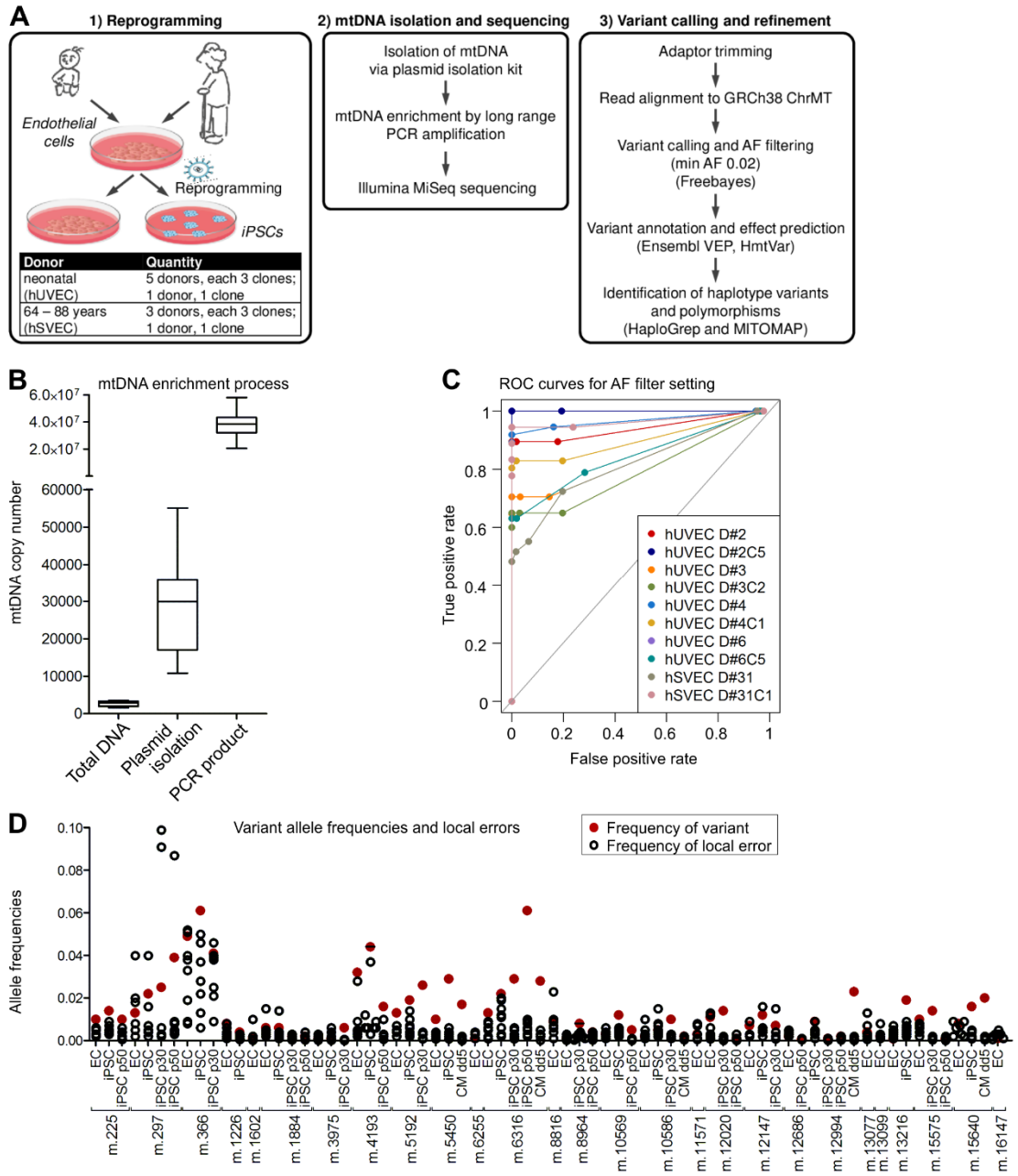

Figure S5: Establishment of our mtDNA sequencing approach; Related to Experimental Procedures section. A Workflow including cell reprogramming, sequencing and sequencing data analysis. **B** mtDNA enrichment by plasmid isolation and long-range PCR amplification for mtDNA sequencing. mtDNA copy number is measured relative to gDNA copy number after total DNA isolation, which represents normal cellular proportion of mtDNA and gDNA, after plasmid isolation, and after additional long range PCR amplification of mtDNA. N = 12. **C** Receiver operating characteristic (ROC) curve with AF as discrimination threshold (AF 0.005, AF 0.01, AF 0.02, AF 0.04, AF 0.06, AF 0.08, AF 0.1, AF 0.5, AF 1). **D** A choice of variants with very low variant allele frequencies in iPSC clones and/or parental cells were additionally investigated individually within their genetic context by inspecting and counting sequencing reads directly. The plot shows the AF of single nucleotide variants (SNVs), calculated from the number of reads with variant, in red against the background of reads with the non-reference and invariant nucleotide exemplarily for 27 loci.

Table S1: Variants detected by mtDNA sequencing; Related to Table 1. List of all variants detected by mtDNA sequencing of 26 iPSC clones at early passage (on average p6.5), of additional 7 of the iPSC clones at intermediate (p30) and high (p50) passage, of the 10 corresponding parental cell populations, and cardiomyocytes differentiated off 4 of the iPSC clones during differentiation process at differentiation day (dd) 0, dd5, and dd15. Variants were divided into groups and categories: Variants of group A, non-transmitted variants, were detected only in parental cell populations. Group B variants were homoplasmic in parental cell population and iPSCs derived thereof. Group C, heteroplasmic variants were detected in an iPSC clone with AF > 0.02 at any passage but were less frequent in the corresponding parental cell population. A final group comprises variants found heteroplasmic in differentiated cardiomyocytes. Those variants basically belong to the group of heteroplasmic variants that were transmitted to cardiomyocytes during differentiation. Variants of category 1 are haplotype variants defining a haplogroup. Category 2 variants are polymorphisms and defined by a population variant frequency (MITOMAP (NCBI GenBank)) ≥ 0.02. Category 3 variants are donor-specific variants which were unique to a donor and rare in the population context. heteroplasmic variants were further divided into the groups of amplified variants (which increase in heteroplasmy level of > 10 fold during iPSC culture expansion), stable variants (with fold change ~1), purified variants (decreased by > 10 fold), fluctuating variants (change of heteroplasmy level did not allow confident classification in one of the above mentioned groups), and "nd in p30-50" variants (iPSC clones not analyzed in high passages). Identification of haplotype variants and polymorphisms was based on HaploGrep, NCBI GenBank variant frequency (obtained from MITOMAP), and HmtVar. Variant effect prediction was performed, based on a consensus of *in silico* prediction algorithms obtained from snpEff impact, CADD, Condel, and HmtVar. The output of each tool for each variant is presented in the respective columns and variants classified as putatively actionable by a harmful designation by snpEff (high impact which indicates frame shift mutations) or at least by two of the other algorithms are marked in red in the consensus column. A choice of variants with very low variant allele frequencies in iPSC clones and/or parental cells were additionally investigated individually within their genetic context by inspecting and counting sequencing reads directly. Variant allele frequencies that were determined using this method are underlined in yellow. (); existence of variant in parental cell population or iPSC clone not confirmed with statistical confidence (p-value > 0.05).

Supplemental excel file

Table S2: Manual determination of very low variant allele frequencies; Related to Experimental Procedures section and mentioned in first Result section.
A Manual determination of very low variant allele frequencies of single nucleotide variants (SNVs). The table lists SNVs and their allele frequencies in iPSC clones and parental cell population determined by individual examination of variants within their genetic context. Results are displayed as the number of reads per respective nucleotide embedded in an 11bp sequence. The number for reference allele reads are given in bold, and for variant allele reads in red. Average local error rates calculation and results, statistical test results, as well as local detection limits are presented.
B Manual determination of very low variant allele frequencies of small insertions. The table lists the small insertions and their allele frequencies in iPSC clones and parental cell population determined by individual examination of variants within their genetic context. Results are displayed as the number of reads for the reference (bold) and variant sequence (red) embedded in an 11bp sequence.

Supplemental excel file

Table S3: Karyotype analysis of parental cells and iPSC clones; Mentioned in second Result section.

Sample	Karyotype	Sample	Karyotype	
Neonatal donors				
Parental cells		**iPSC clones**		
			Early passage (~p8)	**Late passage (~p52)**
D#1 hUVEC	46,XX[15]	**D#1 hUVEC C2**	46,XX[10]	Not analyzed
		D#1 hUVEC C5	46,XX[10]	Not analyzed
		D#1 hUVEC C6	46,XX[10]	Not analyzed
D#2 hUVEC	46,XX[15]	**D#2 hUVEC C4**	46,XX[10]	Not analyzed
D#3 hUVEC	46,XX[15]	**D#3 hUVEC C1**	46,XX[15]	46,XX[20]
		D#3 hUVEC C2	Not analyzed	46,XX[15]
D#4 hUVEC	Not analyzed	**D#4 hUVEC C1**	46,XY[15]	Not analyzed
D#5 hUVEC	Not analyzed	**D#5 hUVEC C1**	46,XX[12]	Not analyzed
D#6 hUVEC	Not analyzed	**D#6 hUVEC C2**	46,XY[12]	Not analyzed
Aged donors				
Parental cells		**iPSC clones**		
			Early passage (~p8)	**Late passage (~p52)**
D#31 hSVEC (64 years)	47,XY,+12[3] / 46,XY,del(13)(q21q31)[2] / 46,XY[10]	**D#31 hSVEC C1**	47,XY,+12[10] / 46,XY[3]	Not analyzed
		D#31 hSVEC C3	47,XY,+12[13] / 48,idem,+mar[2]	Not analyzed
		D#31 hSVEC C4	47,XY,+12[14]	Not analyzed
D#37 hSVEC (73 years)	46,XY[10]	**D#37 hSVEC C8**	46,XY[10]	Not analyzed
		D#37 hSVEC C10	Not analyzed	46,XY[26]
D#38 hSVEC (88 years)	46,XY[10]	**D#38 hSVEC C5**	46,XY[10]	Not analyzed
		D#38 hSVEC C6	46,XY[10]	Not analyzed
		D#38 hSVEC C9	46,XY[10]	Not analyzed
D#40 hSVEC (79 years)	46,XY[10]	**D#40 hSVEC C4**	46,XY[10]	Not analyzed

Table S4: Primer list; Related to Experimental Procedures section. Primer sequences for mtDNA copy number determination by qRT-PCR and whole mtDNA amplification for mtDNA sequencing.

Gene symbol	Primer Forward sequence	Primer Reverse sequence	Product length	Annealing (°C)	Application	Source
LYZL4	GGC CTT CTT ATT GCT GAG GTT C	TAG TCT TCT CCC TTC CTG TCT GC	123	66	Copy number	
PTBP2	TCT CCA TTC CCT ATG TTC ATG C	GTT CCC GCA GAA TGG TGA GGT G	114	65	Copy number	
GKN2	TGC TGA CCA TCT TTG GGA TAC	TTC AGG CTC TCT TGT ACC TTC C	112	60	Copy number	
mtDNA 8294	CCA CTG TAA AGC TAA CTT AGC ATT AAC C	GTG ATG AGG AAT AGT GTA AGG AGT ATG G	143	63	Copy number	Andréasson, BioTechniques. 2002
RNR2	CGT TCA AGC TCA ACA CCC ACT AC	GTT TTA ATC TGA CGC AGG CTT ATG	156	62	Copy number	
ND1	ATA CCC ATG GCC AAC CTC CTA C	TTC ATA GTA GAA GAG CGA TGG TGA GAG	259	62	Copy number	Wurmb-Schwark, Forensic Sci Int. 2002
F2480A/R 10858A	AAA TCT TAC CCC GCC TGT TT	AAT TAG GCT GTG GGT GGT TG	8379	54	Whole mtDNA amplification	McElhoe, Forensic Sci Int Genet. 2014
F10653B/ R2688B	GCC ATA CTA GTC TTT GCC GC	GGC AGG TCA ATT TCA CTG GT	8605	54	Whole mtDNA amplification	McElhoe, Forensic Sci Int Genet. 2014
PINK1	GGA CGC TGT TCC TCG TTA	ATC TGC GAT CAC CAG CCA	218	63	Gene expression	Gegg, PLOSone. 2009
PRKN	GCA TCT TCC AGC TCA AGG AG	CTT TTC TCC ACG GTC TCT GC	165	64	Gene expression	Li, J Clin Med. 2018
Mfn1	TGT TTT GGT CGC AAA CTC TG	CTG TCT GCG TAC GTC TTC CA	160	56	Gene expression	Cartoni, J Physiol. 2005
OPA1	GTG CTG CCC GCC TAG AAA	AGA CTG GCA GAC CTC ACA GG	282	65	Gene expression	
DNM1L	AGG AAG GAG GCG AAC TGT G	TGC TCT GCG TTC CCA CTA C	185	65	Gene expression	
POLG2	GCA GTC CTC ATT GGA ACA ACT	TTG TGG TGT CTC TGC TTC TCA	122	60	Gene expression	
TFAM	ATG GCG TTT CTC CGA AGC AT	CAG ATG AAA ACC ACC TCG GTA A	133	61	Gene expression	Prigione, Stem cell. 2010
NRF1	AAC AAA ATT GGG CCA CGT TAC A	TCT GGA CCA GGC CAT TAG CA	291	62	Gene expression	Prigione, Stem cell. 2010
PRKAA1	CAG CCG AGA AGC AGA AAC AC	TTT GCC AAC CTT CAC TTT GC	101	60	Gene expression	
PGC1A	TCA GTC CTC ACT GGT GGA CA	TGC TTC GTC GTC AAA AAC AG	351	61	Gene expression	Cartoni, J Physiol. 2005
ND5	TAT GTG CTC CGG GTC CAT C	CAG GGA GGT AGC GAT GAG AG	235	63	Gene expression	Amstrong, Stem cell. 2010
PINK1	GGA CGC TGT TCC TCG TTA TG	GGA TGT TGT CGG ATT TCA GG	171	65	Gene expression	adapted Gegg, PLOSone. 2009
PDK1	TTC GGA TCA GTG AAT GCT TG	ACC AAT TGA ACG GAT GGT GT	137	56	Gene expression	Vengellur, Physiol genomics. 2005
mTOR	AGG CCG CAT TGT CTC TAT CA	GCA GTA AAT GCA GGT AGT CAT CC	80	62	Gene expression	adapted Lv, Cell Physiol Biochem. 2017
PGC1B	CCT TGT GTT AAG GCG GAC AG	CCG AGG TGA GGT GCT TAT GTA G	157	62	Gene expression	
Mfn2	ATG CAT CCC CAC TTA AGC AC	CCA GAG GGC AGA ACT TTG TC	301	62	Gene expression	Cartoni, J Physiol. 2005
ß-MHC	GGC ACA GCC ATG GGA GAT TC	TCG AAC TTG GGT GGG TTC TGC	263	60	Gene expression	
α-MHC	CCG TGA AGG GAT AAC CAG GGG	ACT TGG GTG GGT TCT GCT GC	281	60	Gene expression	
PLN	GCT GCC AAG GCT ACC TAA AAG	GAC GTG CTT GTT GAG GCA TTT	182	60	Gene expression	
RYR2	AGA ACT TAC ACA CGC GAC CTG	CAT CTC TAA CCG GAC CAT ACT GC	199	60	Gene expression	
Troponin (TNNT2)	TTC ACC AAA GAT CTG CTC CTC GCT	TTA TTA CTG GTG TGG AGT GGG TGT GG	166	60	Gene expression	
CX43	Gap junction protein, alpha 1, 43kDa (Bio Rad; Cat. #10025636)		130	60	Gene expression	
GAPDH	CCA TCT TCC AGG AGC GAG ATC	GCA GAG ATG ATG ACC CTT TTG G	145	61	Gene expression	
RPL13A	CGC CCT ACG ACA AGA AAA AGC	CCT GGT ACT TCC AGC CAA C	123	61	Gene expression	

Table S5: Variants with minimum AF of 0.02 can be detected in sequencing replicates with repetitious accuracy; Related to Experimental Procedures section. Comparison of variant allele frequencies (AF) in early passages (p6) of three iPSC clones (D#3 hUVEC C1, D#3 hUVEC C2, and D#37 hSVEC C10) and in samples of differentiation day (dd) 0 from targeted cardiomyocyte (CM) differentiations of the respective clones (upper part). The dd0 samples of these CM differentiations for which differentiation was initiated at p6 represent basically independent replicates (including separate sample preparation and sequencing) of the sequencing of the corresponding iPSC clones. Absence of substantial variation in the heteroplasmy levels between dd0, dd5, and dd15 samples of CM differentiations of different iPSC clones (lower part) rebuts a role of amplification and sequencing artefacts.

Variants	Donor	iPSC clone	Variant allele frequency		Fold change	delta AF
			p6.5	dd0		
m.12020C>T	D#37 hSVEC	C10	0.026	0.027	1.04	0.00
m.12686T>C	D#37 hSVEC	C10	0.225	0.203	1.11	0.02
m.72T>C	D#3 hUVEC	C2	0.929	0.946	1.02	0.02
m.5192A>C	D#3 hUVEC	C1	0.019	0.027	1.41	0.01
m.5894_5895insC	D#37 hSVEC	C10	0.979	0.971	1.01	0.01
m.13099G>A	D#3 hUVEC	C2	0.374	0.363	1.03	0.01
m.4193T>C	D#3 hUVEC	C1	0.044	0.013	3.49	0.03
m.5450C>T	D#3 hUVEC	C2	0.029	0.020	1.41	0.01

Variants	Donor	iPSC clone	Variant allele frequency			Fold change	delta AF
			dd0	dd5	dd15		
m.72T>C	D#3 hUVEC	C2	0.946	0.948	0.967	0.99	0.01
m.297A>C	D#37 hSVEC	C4	0.071	0.077	0.073	0.98	0.00
m.4193T>C	D#3 hUVEC	C1	0.013	0.010	0.014	0.96	0.00
m.5192A>C	D#3 hUVEC	C1	0.027	0.024	0.022	1.13	0.00
m.5450C>T	D#3 hUVEC	C2	0.020	0.017	0.018	1.11	0.00
m.5894_5895insC	D#37 hSVEC	C10	0.971	0.972	0.967	1.00	0.00
m.6316A>C	D#37 hSVEC	C4	0.032	0.028	0.032	0.99	0.00
m.10569G>A	D#3 hUVEC	C2	0.014	0.016	0.012	1.09	0.00
m.12020C>T	D#37 hSVEC	C10	0.027	0.032	0.028	0.98	0.00
m.12686T>C	D#37 hSVEC	C10	0.203	0.185	0.205	1.00	0.01
m.13099G>A	D#3 hUVEC	C2	0.363	0.358	0.364	1.00	0.00

Table S6: Antibody and dye list; Related to Experimental Procedures section.

Antibody / Dye	Host / Isotype	Dilution	Company	Application
ATPIF1	Mouse IgG1	1:200	Thermo Fisher Scientific	Immunofluorescence
Anti-mouse IgG-Alexa Fluor 488	Donkey	1:200	Jackson ImmunoResearch	Immunofluorescence
DAPI		1:30000	Sigma-Aldrich	Immunofluorescence
MitoTracker		1µM	Invitrogen	Flow cytometry
ROS Brite 670		5µM	Biomol; AAT Bioquest	Flow cytometry
Tetramethylrhodamine (TMRM)		100nM	Thermo Fisher Scientific	Flow cytometry
Sarcomeric α-actinin	mouse IgG1	1:800	Sigma-Aldrich	Flow cytometry
MYH1E (MF20)	mouse IgG2a	1:50	Hybridoma Bank, University of Iowa, US	Flow cytometry
Troponin-T	mouse IgG1	1:100	Richard Allan Scientific	Flow cytometry
Anti-mouse IgG Alexa Fluor 647	Donkey	1:300	Jackson ImmunoResearch	Flow cytometry

Data S1: Galaxy workflows; Related to Experimental Procedures section.

Supplemental file

Supplemental Experimental Procedures:

Reprogramming and iPSC culture. Derivation and culture of endothelial cells, virus production, retroviral reprogramming, iPSC characterization, and culture was performed as previously described (Haase et al., 2009). In short, endothelial cells (ECs) were isolated from umbilical vein (hUVEC) from healthy newborns and saphenous vein (hSVEC) from aged patients (64-88 years) that underwent coronary bypass surgery. Human material was collected after approval by the local Ethics Committee and following the donor's or the newborn's parental written informed consent. ECs were cultivated in Endothelial Growth Medium (EGM-2) (Lonza) and $2*10^5$ cells of early passages (mean p4.5; range p3-7) were reprogrammed by ectopic expression of Oct4, Sox2, Nanog, and Lin28 (lentiviral transduction, monocistronic factors, multiplicity of infection (MOI) 20) with exception of clone D#40 hSVEC C5 which was reprogrammed via ectopic expression of Oct4, Sox2, Klf4, and c-Myc (lentiviral transduction, monocistronic factors, MOI 1). In total, 26 EC-derived iPSC clones were derived from 10 donors. 3 clones were generated for each donor D#1 hUVEC-D#5 hUVEC, D#31 hSVEC, D#37 hSVEC, and D#38 hSVEC. 1 clone was selected for the donors D#6 hUVEC and D#40 hSVEC. iPSC clones were cultivated as colonies on mouse embryonic fibroblasts (MEF) in Knock-out Dulbecco's Modified Eagle's medium (DMEM) (Gibco) supplemented with 20% KnockOut serum replacement, 1% Non-essential Amino acids, 1mM L-Glutamine, 0.1mM β-Mercaptoethanol (all obtained from Life Technologies), and 10ng/ml bFGF (Institute for Technical Chemistry, Leibniz University Hannover, Germany). Before analysis, iPSCs were transferred to monolayer culture on Geltrex (Thermo Fisher Scientific) in in-house Essential 8 (E8) medium (DMEM Nutrient Mixture F-12 (Gibco) supplemented with 543mg/L $NaHCO_3$, 2ng/ml TGFβ (PeproTech), 10.7µg/ml human recombinant transferrin, 14µh/l sodium selenite, 20µg/l insulin, 64µg/l ascorbic acid 2-phosphate (all obtained from Sigma-Aldrich), and 100ng/ml bFGF) and cultured for generally 3-5 passages.

Primer Design for the determination of mitochondrial DNA copy number using quantitative real-time PCR (qRT-PCR). A quantitative real-time PCR (qRT-PCR) based analysis system was developed which quantifies mitochondrial DNA (mtDNA) copy number relative to genomic DNA (gDNA) copy number. In contrast to most other studies which use only one primer pair, our system measures number of mtDNA and gDNA copies by each three primer pairs. Sequences for two primer pairs targeting mtDNA regions were assimilated from previous studies (Andreasson et al., 2002; von Wurmb-Schwark et al., 2002). The other primer pairs were designed employing Primer3 (v0.4.0). During primer design, target loci were chosen that were not within the common 4700bp mtDNA deletion site or genomic regions with high CNVs or mutation occurrence (manually inspected using variation data provided by Ensembl (release 90, August 2017) (Hunt et al., 2018).

mtDNA extraction and amplification. The workflow for mtDNA sequencing and data processing is displayed in Figure S5A. mtDNA was extracted via QIAprep Spin Miniprep kit (Qiagen) from early passage iPSC clones (mean p6.5), and from late passages (p30 and p50) of 7 clones. Furthermore, enriched mtDNA was isolated from the corresponding parental cell populations at a similar passage as subjected to reprogramming (mean p4.5). Isolation was essentially performed according to manufacturer's recommendation and yielded, on average, 12 fold increase of mtDNA compared to total DNA isolation (Figure S5B). Entire mtDNA was then amplified using 2 primer pairs (F2480A/R10858A (3:1) and F10653B/R2688B (1:1)) (Table S4) generating two overlapping PCR products of 8379bp and 8605bp fragment size (McElhoe et al., 2014). PCR reactions were performed with Herculase II Fusion DNA Polymerase (Agilent) in technical replicates with 50ng enriched mtDNA as template per reaction. Altogether, the input of enriched mtDNA accounted for 200ng which equals to ~$5*10^8$ mtDNA molecules ($3.2*10^4$ cells (theoretical input) * 12 (average fold enrichment) * 1300 (average mtDNA copy number per cell)), isolated from, on average, $5*10^6$ iPSCs or $2.5*10^6$ parental cells. PCR conditions were: 94°C for 5min as initiation step, then 23 cycles of 94°C for 40s, 54°C for 20s, and 54°C for 4.15min, followed by termination step of 72°C for 3min. Therefore, our protocol reduced PCR amplification cycle to 23 compared to 30 in most other published approaches of mtDNA amplification for sequencing purposes. mtDNA PCR amplification resulted in an enrichment of mtDNA of, on average, ~15000 fold over normal cellular content (Figure S5B). Each amplicon was individually inspected by gel electrophoresis and amplicons from the same sample were pooled,

Read trimming, quality assessment, and alignment. Quality and adapter trimming of reads was performed by Trim Galore (v0.4.3; Cutadapt v1.14) including removal of adapter, 10bp from the 3' end of read 1, 30bp from the 3' end of read 2, as well as low-quality ends from reads (Phred < 28). Reads were aligned to the human genome GRCh38 chromosome MT (the Cambridge Reference sequence (rCRS; NC_012920)) using BWA-MEM (Galaxy Version 0.7.17.1) (Li, 2013). Quality of trimmed and aligned reads were inspected employing FastQC Read Quality reports (v.0.11.6; Galaxy wrapper version v0.71) and Qualimap Multi-sample BAM QC analysis (v.2.2.1). Reads had an average length of 215bp, with Phred score > 28 over whole read length. 98% of all reads mapped to mitochondrial reference genome with equal quality across the reference genome (59.8 mean mapping quality). The coverage was 19000 on average.

Variant calling and refinement. Variants were called using FreeBayes (v1.0.2; Galaxy implementation v1.0.2.29-3) (Ewing and Green, 1998; Ewing et al., 1998) with filters set to ploidy 10, minimum coverage 100, and minimum AF (alternative frequency) 0.02. The evaluation of the AF filter threshold was performed based on knowledge of population frequency of variants and the high coverage was utilized to identify false and true variants. Variants that were detected at a low frequency in iPSC clones of different donors but were not describe as polymorphism were unlikely to be true-positive. Subsequently some selected variants were individually analyzed as described below in the section "Detection of variants at very low AF". A receiver operating characteristic (ROC) curve with AF as discrimination threshold (Figure S5C) showed that AF 0.02 retrieve very high specificity while maintaining most true positive variants. To exclude the few remaining false positive variants, remaining primer sequences that had evaded the trimming process were manually removed and variants that were detectable in different donors (with minimum AF 0.005) but not described as polymorphisms were excluded as probable false variant calls.

Determination of allele fraction of variants with very low AF in iPSC clones and parental cell population. The presence of a choice of variants (in total 128 variants at 38 different genetic regions) at very low AF (in general, ≤ 0.02) in iPSC clones or parental cell populations was examined individually within their genetic context. For this purpose, sequencing reads were inspected directly from fastq raw files. Both reads of the paired end sequencing were investigated and the number of reads with the variant enclosed by a 11bp long sequence ranging from position -5bp to +5bp was counted as well as the number of reads with the reference sequence. For calculation of average error for each genetic location, the numbers of reads that comprised not the variant or reference nucleotide were determined. In addition, the 11bp long sequences directly upstream and downstream of the variant were analyzed in the same manner. Hence, the average error of the amplicon sequencing was calculated for every variant as the mean number of reads with non-reference and non-variant nucleotide at variant location or in the middle of analyzed upstream and downstream sequence (in general, N = 8) and presence of variant was confirmed with p-value 0.05 against background of errors (Figure S5D, Table S2A). Frequencies of INDELs were determined by extracting and counting reads for both INDEL and reference sequence embedded by an 11bp sequence, directly from fastq files (Table S2B). Average error of the amplicon sequencing was calculated for every variant as the mean number of reads with non-reference and non-variant nucleotide at variant location or in the middle of analyzed upstream and downstream sequence (in general, N = 8). Distribution of errors for each variant was evaluated via the D'Agostino and Pearson omnibus normality test (where applicable, else the Shapiro-Wilk normality test was used). One sample one-tailed t-test and Wilcoxon one-tailed signed-rank test were performed, respectively, to compare number of reads with variant as hypothetical value against background of errors. The null hypothesis, assuming number of reads with variant is within local error range, was rejected with p values of 0.05.

Karyotype analysis. After treatment of hiPSCs with colcemid (Invitrogen) for 30 min, cells were detached with trypsin and metaphases were prepared according to standard procedures. Fluorescence R-banding using chromomycin A3 and methyl green was performed as previously described (Schlegelberger et al., 1999). At least 10 metaphases were analyzed per clone at a minimum of 300 bands. Karyotypes were described according to the international System for Human Cytogenetic Nomenclature (ISCN).

Differentiation of cardiomyocytes (CMs). For CM differentiation, $1*10^6$ undifferentiated cells/well were aggregated in 3ml E8 medium containing 10µM Rho-Kinase inhibitor Y-27632 (RI) on low attachment 6 well plates (Greiner Bio-one GmbH) on an orbital shaker (70rpm; Infors GmbH) at differentiation day (dd) -3). Differentiation was started (dd0) using 5µM CHIR99021 (LU Hannover) in CDM3 (Burridge et al., 2014; Halloin et al., 2019) to activate the WNT pathway. Exactly 24h later it was followed by a subsequent inhibition of the WNT pathway (dd1), where CDM3 medium including 2µM Wnt-C59 (LU Hannover) was added for 48h. On dd3 and dd5 fresh CDM3 medium was added. From dd7 on, the medium was changed to basic serum free medium (bSF; DMEM with 1% non-essential amino acids, 5.6mg/l transferrin, 37.2µg/l sodium-selenit, 1mM L-glutamine, and 10µg/ml insulin) and was changed every other day. The differentiation efficiency was addressed on dd14 by flow cytometry for the cardiac markers, cardiac troponin T (cTnT), alpha sarcomeric actinin (αSA), and pan-myosin heavy chain (MF20) as described earlier (Halloin et al., 2019) (Table S6). mtDNA of $5*10^6$ iPSC-derived cardiomyocytes at dd0, dd5, and dd15 was isolated, amplification, and subjected to sequencing as described above.

Bioartificial cardiac tissues (BCT) generation and cultivation. BCTs were generated and cultivated as described earlier (Kensah et al., 2011; Kensah et al., 2013). Briefly, differentiated CMs were dissociated using STEMdiff™ Cardiomyocyte Dissociation Kit (STEMCELL Technologies) according to manufacturer's instructions. 250µl cell-matrix mixture/BCT composed of 10% Matrigel (BD Biosciences), 1.35mg/ml rat collagen type I (Trevigen), 3.6% 0.4M NaOH, $1*10^6$ dissociated CMs, and $1*10^5$ irradiated human foreskin fibroblasts (ATCC) was poured into bottomless silicon molds containing two titanium rods (6mm initial slack length). Following 30min solidification, the tissues were cultivated in BCT medium with 30µM L-ascorbic acid

(Kensah et al., 2011) for 21 days, where spontaneously contracting BCTs formed around the rods. Starting on day 7, a growing static stretch protocol of 0.4mm/4days was applied. Tissue maturation and CM viability was monitored during cultivation using an AxioObserver Z1 fluorescence microscope and ZEN 3.1 software (Zeiss). To visualize the distribution of viable CMs, the mitochondria-specific dye tetramethylrhodamine methyl ester (TMRM, 25nM; Thermo Fisher Scientific) was added. Active contraction forces and spontaneous beating frequencies of BCTs were measured on day 21 of tissue cultivation as described earlier 53 using a custom-made bioreactor system (Central Research Devices Service Unit, MHH, Hannover). BCTs were placed into a culture vessel (BCT medium, 37°C) allowing for contraction force recording, and precise application of increasing preload. After every preload step (200µm increments), spontaneous and paced contraction (mean of 5 biphasic pulses, 10ms, 25V) values were measured.

Immunofluorescence staining and microscopic analysis. ECs, iPSCs, and CMs were seeded on cover slides coated with 1% gelatin, Geltrex, or 50µg/ml fibronectin in 0.02% gelatin, respectively. After a culture period of 1-2 days for ECs and iPSCs and 3 days for CMs, cells were fixed with 4% Paraformaldehyde (PFA) for 20min at 4°C, permeabilized with 0.1% Triton X 100 (Sigma-Aldrich) in PBS for 5min at room temperature, and unspecific binding sites were blocked with solution of 5% donkey serum (Chemikon) and 0.25% Triton X 100 in tris-buffered saline (TBS) for 30min at 4°C. Incubation with monoclonal anti-ATPIF1 (ATP synthase subunit IF1) antibody diluted in staining buffer (PBS with 1% bovine serum albumin (BSA) (Sigma-Aldrich)) was performed overnight at 4°C. List of antibodies is provided in Table S6. Secondary antibody staining was performed for 1h at 4°C and DAPI nuclear staining for 1min.

Supplemental References:

Andreasson, H., Gyllensten, U., and Allen, M. (2002). Real-time DNA quantification of nuclear and mitochondrial DNA in forensic analysis. Biotechniques *33*, 402-404, 407-411.

Burridge, P.W., Matsa, E., Shukla, P., Lin, Z.C., Churko, J.M., Ebert, A.D., Lan, F., Diecke, S., Huber, B., Mordwinkin, N.M., *et al.* (2014). Chemically defined generation of human cardiomyocytes. Nat Methods *11*, 855-860.

Ewing, B., and Green, P. (1998). Base-calling of automated sequencer traces using phred. II. Error probabilities. Genome Res *8*, 186-194.

Ewing, B., Hillier, L., Wendl, M.C., and Green, P. (1998). Base-calling of automated sequencer traces using phred. I. Accuracy assessment. Genome Res *8*, 175-185.

Haase, A., Olmer, R., Schwanke, K., Wunderlich, S., Merkert, S., Hess, C., Zweigerdt, R., Gruh, I., Meyer, J., Wagner, S., *et al.* (2009). Generation of induced pluripotent stem cells from human cord blood. Cell Stem Cell *5*, 434-441.

Halloin, C., Schwanke, K., Lobel, W., Franke, A., Szepes, M., Biswanath, S., Wunderlich, S., Merkert, S., Weber, N., Osten, F., *et al.* (2019). Continuous WNT Control Enables Advanced hPSC Cardiac Processing and Prognostic Surface Marker Identification in Chemically Defined Suspension Culture. Stem Cell Reports *13*, 366-379.

Hunt, S.E., McLaren, W., Gil, L., Thormann, A., Schuilenburg, H., Sheppard, D., Parton, A., Armean, I.M., Trevanion, S.J., Flicek, P., *et al.* (2018). Ensembl variation resources. Database *2018*.

Kensah, G., Gruh, I., Viering, J., Schumann, H., Dahlmann, J., Meyer, H., Skvorc, D., Bar, A., Akhyari, P., Heisterkamp, A., *et al.* (2011). A novel miniaturized multimodal bioreactor for continuous in situ assessment of bioartificial cardiac tissue during stimulation and maturation. Tissue Eng Part C Methods *17*, 463-473.

Kensah, G., Roa Lara, A., Dahlmann, J., Zweigerdt, R., Schwanke, K., Hegermann, J., Skvorc, D., Gawol, A., Azizian, A., Wagner, S., *et al.* (2013). Murine and human pluripotent stem cell-derived cardiac bodies form contractile myocardial tissue in vitro. European Heart Journal *34*, 1134-1146.

McElhoe, J.A., Holland, M.M., Makova, K.D., Su, M.S., Paul, I.M., Baker, C.H., Faith, S.A., and Young, B. (2014). Development and assessment of an optimized next-generation DNA sequencing approach for the mtgenome using the Illumina MiSeq. Forensic Sci Int Genet *13*, 20-29.

Schlegelberger, B., Metzke, S., Harder, S., Zühlke-Jenisch, R., Zhang, Y., and Siebert, R. (1999). Classical and Molecular Cytogenetics of Tumor Cells. In Diagnostic Cytogenetics, R.-D. Wegner, ed. (Berlin, Heidelberg: Springer Berlin Heidelberg), pp. 151-185.

von Wurmb-Schwark, N., Higuchi, R., Fenech, A.P., Elfstroem, C., Meissner, C., Oehmichen, M., and Cortopassi, G.A. (2002). Quantification of human mitochondrial DNA in a real time PCR. Forensic Sci Int *126*, 34-39.